Vibration-based Bayesian model updating of civil engineering structures applying Gaussian process metamodel

Vibration-based Bayesian model updating of civil engineering structures applying Gaussian process metamodel

Journal:	*Advances in Structural Engineering*
Manuscript ID	ASE-18-0610.R2
Manuscript Type:	Special Issue for Prof JM Ko
Date Submitted by the Author:	19-May-2019
Complete List of Authors:	Moravej, Hossein; Queensland University of Technology Faculty of Science and Engineering, Civil Engineering & Built Environment Chan, Tommy Nguyen, Khac Duy; Queensland University of Technology Faculty of Science and Engineering, Civil Engineering & Built Environment Jesus, Andre; University of West London, School of Computing and Engineering
Keywords:	Finite Element Model Updating, Bayesian framework, Gaussian process, Structural Health Monitoring, Box girder bridge, Vibration analysis
Abstract:	Structural health monitoring plays a significant role in providing information regarding the performance of structures throughout their life spans. However, information that is directly extracted from monitored data is usually susceptible to uncertainties and not reliable enough to be used for structural investigations. Finite element model updating (FEMU) is an accredited framework that reliably identifies structural behavior. Recently, the modular Bayesian approach (MBA) has emerged as a probabilistic technique in calibrating the finite element model (FEM) of structures and comprehensively addressing uncertainties. However, few studies have investigated its performance on real structures. In this paper, MBA is applied to calibrate the FEM of a lab-scaled concrete box girder bridge. This study is the first to use the MBA to update the initial FEM of a real structure for two states—undamaged and damaged conditions—in which the damaged state represents changes in structural parameters as a result of aging or overloading. The application of the MBA in the two states provides an opportunity to examine the performance of the approach with observed evidence. A discrepancy function is used to identify the deviation between the outputs of the experimental and numerical models. To alleviate computational burden, the numerical model and the model discrepancy function are replaced by Gaussian processes. Results indicate a significant reduction in the stiffness of concrete in the damaged state, which is identical to cracks observed on the body of the structure. The discrepancy function reaches satisfying ranges in both states, which implies that the properties of the structure are predicted accurately. Consequently, the proposed methodology contributes to a more reliable judgment about structural safety.

Vibration-based Bayesian model updating of civil engineering structures applying Gaussian process metamodel

Hossein Moravej, Tommy Chan, Khac-Duy Nguyen and

Andre Jesus

Abstract

Structural health monitoring plays a significant role in providing information regarding the performance of structures throughout their life spans. However, information that is directly extracted from monitored data is usually susceptible to uncertainties and not reliable enough to be used for structural investigations. Finite element model updating (FEMU) is an accredited framework that reliably identifies structural behavior. Recently, the modular Bayesian approach (MBA) has emerged as a probabilistic technique in calibrating the finite element model (FEM) of structures and comprehensively addressing uncertainties. However, few studies have investigated its performance on real structures. In this paper, MBA is applied to calibrate the FEM of a lab-scaled concrete box girder bridge. This

study is the first to use the MBA to update the initial FEM of a real structure for two states—undamaged and damaged conditions—in which the damaged state represents changes in structural parameters as a result of aging or overloading. The application of the MBA in the two states provides an opportunity to examine the performance of the approach with observed evidence. A discrepancy function is used to identify the deviation between the outputs of the experimental and numerical models. To alleviate computational burden, the numerical model and the model discrepancy function are replaced by Gaussian processes. Results indicate a significant reduction in the stiffness of concrete in the damaged state, which is identical to cracks observed on the body of the structure. The discrepancy function reaches satisfying ranges in both states, which implies that the properties of the structure are predicted accurately. Consequently, the proposed methodology contributes to a more reliable judgment about structural safety.

Keywords

Finite Element Model Updating, Bayesian framework, Gaussian process, Structural Health Monitoring, Box girder bridge, Vibration analysis

Introduction

Civil infrastructure plays a significant role in keeping urban systems operational, but any malfunctions in routine performance can result in major hazards and even threaten lives. Therefore, it is important to regularly investigate the safety of infrastructure. Many researchers such as Frangopol (2011) and Li et al. (2016) have acknowledged the importance of monitoring the behaviors of structures using information provided by structural health monitoring (SHM). An accredited approach to addressing the aforementioned objective is finite element model updating (FEMU), which aims to improve the accuracy of the finite element models (FEMs) of real structures and reduce the discrepancy between the output of FEMs and experimental measurements. The availability of reliable FEMs of structures is beneficial in terms of evaluation of structural performance, reliability analysis, load-carrying capacity assessment, and damage detection.

However, FEMU faces significant barriers that prevent it from reaching its peak efficiency. For example, computational burden, especially in the case of complex structures, makes this technique cumbersome, and in some cases, the process of updating may lead to ill-conditioned optimization problems with limited practical applicability. Although some approaches have recently been introduced to improve computational efficiency, such as the response surface method (Shahidi and Pakzad,

2013) and the substructure technique (Weng et al., 2012), this challenge still needs to be addressed.

Another challenge when updating a model relates to addressing different sources of uncertainties. To overcome this problem, probabilistic approaches that are more reliable than their deterministic counterparts have been introduced in the field of FEMU (Jesus et al., 2014; Jesus et al., 2018). Deterministic techniques, which consider fixed values regarding input parameters and response outputs, rarely provide a satisfactory correlation between the numerical model and real data because of inherent structural uncertainties (Friswell and Mottershead, 2013). In contrast, probabilistic approaches do not regard input parameters as fixed numbers to lock the updating process in those values; instead, they consider a realistic statistical distribution for each parameter. This consideration is more logical because it is impossible to confidently assert a certain value for one parameter using an updating process because of the existence of uncertainties. Therefore, in most cases, probabilistic approaches are more reliable. According to Kennedy and O'Hagan (2001a, 2001b), the main sources of uncertainty in model prediction are uncertainty in model parameters, modeling errors, and uncertainty resulting from observation errors. Uncertainty in model parameters relates to inputs to the computer model that are unknown and cannot be identified directly from physical experiments, such as the material properties of a damaged structure. Another source

of uncertainty—modeling error or model inadequacy—refers to any assumptions or simplifications made while developing FEMs, such as considering a material linear, isotropic, and homogenous. This source of uncertainty occurs even when all parameters are accurately identified. The observation error (i.e., experimental uncertainty) is usually present in physical experiments. This type of uncertainty denotes variations that may occur in the experimental measurement even when the test is repeated with the same settings.

Despite the significant effects of the abovementioned uncertainties, few studies have addressed all of these aspects. A number of probabilistic approaches have been developed in FEMU, including the fuzzy number-based method, Kalman Filter-based technique, model falsification diagnosis method, Markov process-based method and sampling method. Among all probabilistic FEMU techniques, Bayesian updating has been found to be one of the most applicable approaches for updating FEMs. Several attempts have been made to apply Bayesian updating, and Beck's method is eminent among them because it proposes a robust predictive approach (Beck and Katafygiotis, 1998; Beck and Au, 2002). The major weakness in the presentation of Bayesian methods in SHM practices is that uncertainty resulting from modeling errors is not properly considered. Only a few researchers have performed the Bayesian approach with consideration of this aspect (Higdon et al., 2008; Simoen et al., 2013). Higdon used a comprehensive modular Bayesian

approach (MBA) that was formerly established by Kennedy and O'Hagan (2001a), but it was not generally successful in addressing identifiability. Identifiability represents the ability to achieve the true value of model parameters based on available data to illustrate a physical property such as Young's modulus (Arendt et al., 2012a). Arendt et al. (2012b) proposed an improvement to Kennedy and O'Hagan's original formulation using the MBA to overcome the identifiability problem by applying measured data with various responses. This method replaces an FEM with a Gaussian process (GP) model as a metamodel (Kennedy and O'Hagan, 2001a). It has been found that the method significantly reduces computational effort—especially in cases of complex structures (Lophaven et al., 2002; Jesus et al., 2017; Conde et al., 2019; Jesus et al., 2019). The GP model for interpolation that considers uncertainties is found to be effective, even if data are limited. This formulation is preferable to former studies in model updating because it comprises the main sources of uncertainties and consequently reaches more realistic outcomes.

Based on the thriving interest in the MBA, this study validates its practical performance in FEMU by means of measured vibration data. The study investigates the applicability of the algorithm to a lab-scaled reinforced concrete box girder bridge (BGB), which represents a typical hollow core bridge deck in Australia. The MBA is applied in two states—undamaged and damaged—to calibrate multiple

parameters of the FEM. The performance of the approach is examined according to the observed evidence of the undamaged condition with initial minor cracks and the damaged condition with imposed cracks. The damaged state represents changes in structural parameters as a result of aging or overloading. Accordingly, this study aims to identify changes in the structural parameters and provide a reliable updated model for each state. The structural identification provided through the applied framework will not only provide a better understanding of structural performance, but will also contribute to providing suitable guidelines for decision-making regarding maintenance actions.

Model Updating Methodology

This section describes the model updating approach used in this study. The first subsection explains the connecting equation between the observations and the outputs of the numerical model. The second subsection briefly presents the GP, and the last subsection outlines the framework.

Observation and numerical model relationship

We assume that a real and unobservable process f has n observations of q responses $\mathbf{Y^e}$ from the measured data, where the superscript "**e**" is the experimental model. The relationship between $\boldsymbol{f}$ and $\mathbf{Y^e}$ can be denoted as equation (1):

$$\mathbf{Y^e} = \boldsymbol{f} + \varepsilon \quad (1)$$

where $\varepsilon = [\varepsilon_1, \ldots, \varepsilon_n]^T$ is the observation error, which is supposed to work as a Gaussian distribution with a mean of 0 and variance of $\Lambda \in \mathbb{R}$. Alternatively, the real process f can be interpreted as equation (2) to comprise the numerical model:

$$\boldsymbol{f} = \mathbf{Y^m}(\theta^*) + \boldsymbol{\delta} \quad (2)$$

where $\boldsymbol{\delta}$ is a discrepancy function that represents the difference between the numerical model and the real process. $\mathbf{Y^m}(\theta^*)$ is the numerical model's output and θ^* is an r-dimensional vector of the true structural parameters. This equation is an idealized form of the final model (i.e., the model after successful calibration), while the model parameters θ take the values θ^*. Significantly, the discrepancy function

does not depend on the model's output and is an unknown in addition to the structural parameters. Equation (2) is then substituted into equation (1) to obtain equation (3):

$$\mathbf{Y^e} = \mathbf{Y^m}(\theta^*)+\boldsymbol{\delta}+\varepsilon \quad (3)$$

Equation (3) is a comprehensive equation of the model updating process. It denotes the output of the processes within the domain of a calibrated status $\theta = \theta^*$, which implies the best fit compared with the observed data.

In the next step, the numerical model and the discrepancy function are substituted with two multiple-response Gaussian processes (MRGPs) whose hyperparameters must be found. These hyperparameters describe the MRGPs and illustrate the approximation of their associated uncertainties such as variability of the numerical model, modeling discrepancies, and observation errors.

Gaussian Process

Gaussian processes (GP) modeling is an interpolation approach that considers uncertainty highly efficient even when data are limited (Kennedy and O'Hagan, 2001a; Rasmussen et al., 2006). By applying interpolations and extrapolations, this

approach offers a predicted GP that is fitted on all observation points. In this study, an MRGP is applied by assuming that the metamodel of model **Y** is a single realization of a spatial random process with a prior mean function and covariance function (O'Hagan, 2006; Rasmussen et al., 2006). Regarding approximation of the metamodel, it is assumed that a dataset of **Y** with a size of g and N observations should be available as input. Dimension g represents the number of responses (Y_1, Y_2,..., Y_g). To generate the MRGP, the mean function is required to be obtained, which exists at every design input point without uncertainty. In the spaces located between or outside the design input points, the MRGP will produce either a possible interpolation or extrapolation from the existing data points.

In the MRGP, the prior mean function is supposed to be a member of a hierarchical structure of linear functions. It can be generalized as the form $\mathbf{M}=\mathbf{H}\boldsymbol{\beta}$. Herein, matrix **H** comprises N polynomial constant regression functions and the matrix of regression coefficient $\boldsymbol{\beta}$ for each term included in matrix **H** and each fitted response in **Y**. That is, **H** is a row vector of regression functions and $\boldsymbol{\beta}$ is a column vector of regression functions.

The prior covariance function of the MRGP for the model and discrepancy function can be formulated as equation (4):

$$\mathbf{V} = \sum^2 \otimes \mathbf{R} \quad (4)$$

where $\mathbf{V}$ is covariance function, $\sum^{\mathbf{2}} \in \mathbb{R}^{g \times g}$ is a non-temporal variance matrix, and $\mathbf{R} \in \mathbb{R}^{N \times N}$ is a temporal correlation matrix, and $\otimes$ is the Kronecker product operation on the two matrices. This equation can be interpreted as the separation of a variance between the g responses (which are being approximated) and a correlation between the N times histories. Each entry of Matrix $\mathbf{R}$ contains a correlation function that needs to be approximated. This assumption is applicable to the correlation function of the numerical model. In addition, because the FEM is linear, a linear correlation function is assumed for the correlation function in this study, as shown in equation (5). This model fits properly to the data and is numerically stable (Lophaven et al., 2002).

$$\mathbf{R}(\omega, \theta, \theta') = \prod_{j=1}^{r} \max\{0, 1 - \omega_j |\theta_j - \theta'_j|\} \quad (5)$$

In equation (5), ω_j ($j=1,...,r$) is the roughness parameter and represents how roughly the responses change from point θ to point θ' for each of the structural parameters of interest.

In contrast, the correlation matrix for the discrepancy function is simply assumed as an identity matrix as **R**=**I**. This assumption implies that the final predicted responses have no temporal correlation. This is reasonable for natural frequencies obtained from a laboratory model because they vary randomly without any definite relations. The final hyperparameter that needs to be estimated to conclude the description of the MRGP is Λ as the $N\times1$ variance vector of the observation error ε, which can simply be added to equation (4) to reach equation (6).

$$\mathbf{V} = \sum^2 \otimes \mathbf{R} + \Lambda \tag{6}$$

After providing a certain amount of data **Y**, the MRGP is provided (supposing a non-informative prior for $\boldsymbol{\beta}$ and given ω and $\sum$). The posterior distribution of the response is given by equation (7):

$$y \mid \boldsymbol{\Sigma}, \omega, \Lambda, \mathbf{Y} \sim N(m^*, \boldsymbol{\Sigma} \otimes \gamma^*) \tag{7}$$

with

$$m^* = h\hat{\boldsymbol{\beta}} + \gamma^{\mathrm{T}} \boldsymbol{\Gamma}^{-1} (\mathbf{Y} - \mathbf{H}\hat{\boldsymbol{\beta}}) \tag{8}$$

$$\mathbf{\gamma}^{*} = \mathbf{\gamma} - \mathbf{\gamma}^{\mathbf{T}}\,\mathbf{\Gamma}^{-1}\,\mathbf{\gamma} + [h^{T} - \mathbf{H}^{\mathbf{T}}\,\mathbf{\Gamma}^{-1}\,\mathbf{\gamma}]^{\mathrm{T}}\,[\mathbf{H}^{\mathbf{T}}\,\mathbf{\Gamma}^{-1}\,\mathbf{H}]^{-1}\,[h^{T} - \mathbf{H}^{\mathbf{T}}\,\mathbf{\Gamma}^{-1}\,\mathbf{\gamma}] \quad (9)$$

where y represents the MRGP, h is the hierarchical structure of regression functions. $\mathbf{\gamma}$ is defined as a relational correlation matrix, which maps the correlation between the indices of points of available dataset and the indices of points supposed to be predicted (Conti et al., 2009). The used correlation function is the same as equation (5). $\hat{\boldsymbol{\beta}}$ stands for the estimated matrix of $\boldsymbol{\beta}$ and is given by calculating equation (10):

$$\mathbf{H}^{\mathbf{T}}\,\mathbf{R}^{-1}\,\mathbf{H}\hat{\boldsymbol{\beta}} = \mathbf{H}^{\mathbf{T}}\,\mathbf{R}^{-1}\,\mathbf{Y} \quad (10)$$

which refers to the linear regression solution of the best linear unbiased predictor. $\mathbf{\Gamma}$ is an $N \times N$ correlation matrix that contains the linear functions. The MRGP in equation (7) can be defined by estimating the hyperparameters ω, $\boldsymbol{\beta}$, $\sum$, and Λ. Characterization of the hyperparameters can be conducted using a Bayesian approach, which would address all of the mentioned uncertainties and identify all of the hyperparameters at the same time. However, this approach is not efficient because it comprises a huge computational process (Liu et al., 2009). Therefore, for better computational efficiency, the hyperparameters are calculated with the

maximum likelihood estimations (MLEs). A more comprehensive description of the GP method can be found in Arendt et al. (2012a).

Modular Bayesian approach (MBA)

The MBA separates the updating process into four steps. The hyperparameters of the MRGP are approximated separately and consecutively, as shown in Figure 5 in the study by Arendt et al. (2012a). In the MBA, the hyperparameters continue to be estimated until the first order of uncertainties is found, and then they are fixed. It is worth noting that setting up the hyperparameters at fixed estimations decreases the degree of approximation of the uncertainties. In addition, the "second-order" resolution of the uncertainties is ignored to alleviate the computational burden and make it faster than fully considering the uncertainties in the Bayesian framework. This act of estimating and fixing the hyperparameters is performed sequentially when progressing from module 1 to module 2 and from module 2 to module 3.

The first module basically substitutes the computer model to an MRGP model and estimates its hyperparameters based on only the simulation data. In this module, the simulation is run in finite element modeling software (e.g., Abaqus) to obtain the simulated responses by randomly changing the input parameters using Latin hypercube sampling (LHS). For the experimental validation in this study, 120 and 80 runs were conducted in the undamaged and damaged states, respectively, to

provide a dataset. The estimation can be carried out using numerical optimization methods by fitting a likelihood between the MRGP and the available simulation data. In this study, a genetic algorithm (GA) routine was applied in MATLAB. For the GA setup, an initial population of size 40 is generated in the [0; 1] range, a Gaussian mutation function with a scale of 1 (i.e., initial standard deviation of 1) and a standard deviation shrink of 1 is chosen, and a scattered crossover function applied to a portion of 0.8 of the population at each generation is defined. Convergence criteria are set as either a maximum number of 100 generations or until an average change in the fitness value of 1×10^{-6} is reached.

In module 2, the discrepancy function is estimated by fitting another MRGP model according to the measured data from the experiment, the simulation data, and the prior distribution of the calibration parameters. The GA is used to approximate the discrepancy function by estimating the hyperparameters of the GP. This task is carried out by an MLE, which indicates that the fitness function of the GA is a likelihood function. It should be mentioned that either the MBA or the full Bayesian approach can estimate the hyperparameters of the abovementioned MRGP models through MLE and Bayesian posterior distributions, respectively. As discussed in the previous section, the MBA is used in this study because Bayesian posterior distributions can be computationally inefficient. In addition, according to Bayarri

et al. (2007), both approaches have similar results in predicting the discrepancy function and calibration parameters.

In module 3, Bayes' theorem is applied to approximate the posterior distribution of the updated parameters and its likelihood function containing the two MRGP models approximated in modules 1 and 2. Since multiple parameters are calibrated in this study, a Markov chain Monte Carlo method can be used to estimate the MBA. This choice implies that a target distribution must be used, and in this study, a multivariate normal distribution is chosen (Arendt et al., 2012b).

In module 4, the experimental responses are calculated by applying the measured data and the estimated hyperparameters obtained from modules 1 and 2. After the simulated and measured data are collected in modules 1 and 2 and the calibrated parameters are estimated in module 3, the posterior distribution response of the updated model together with the updated discrepancy function can be obtained. For the prediction of the responses, 40 measured data points for the undamaged state and 60 data points for the damaged state are randomly distributed along the simulated data points. It is worth noting that simulated data have been provided by applying the LHS approach as described in the first module. In addition, it is assumed that the measured responses are independent of time, temperature variation, and other operational effects.

Finite element model updating for a box girder bridge

The first subsection presents details of the BGB and two different states (i.e., undamaged and damaged) of the structure. Details of an FEM and experimental modal analysis as two counterparts in model updating are provided in the second and third subsections, respectively. The fourth subsection highlights sensitivity analysis as a tool to select appropriate parameters and responses in FEMU.

Two states of box girder bridge

A downscaled reinforced concrete BGB, which was constructed in the civil engineering laboratory at the Queensland University of Technology, is investigated in this study. This structure represents a typical in-service hollow core bridge deck in Australia. The length of the BGB is 6 m, and it was cast in three separate parts as the bottom slab, the webs, and the top slab. Detailed dimensions of the structure are shown in Figure 1 (a). Further information about the casting steps can be found in Pathirage (2017). The BGB was placed on two simple supports as a pin at one end and a roller at the other end, as shown in Figure 1 (b). This platform refers to

the undamaged state (first state), despite the existence of some minor cracks beneath the soffit slab.

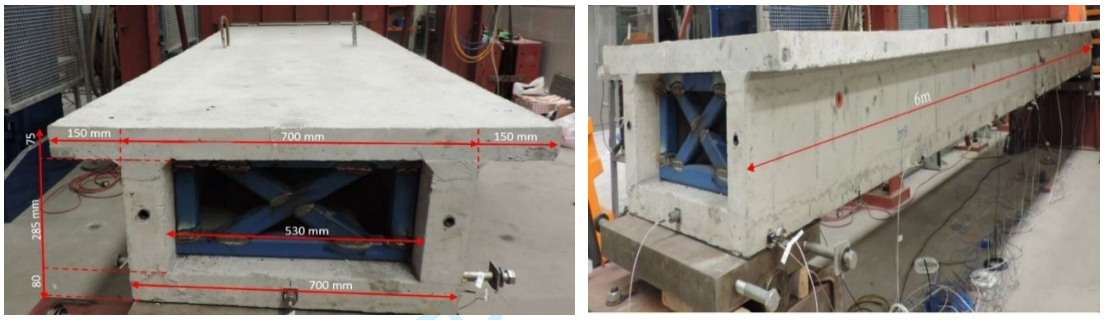

(a)

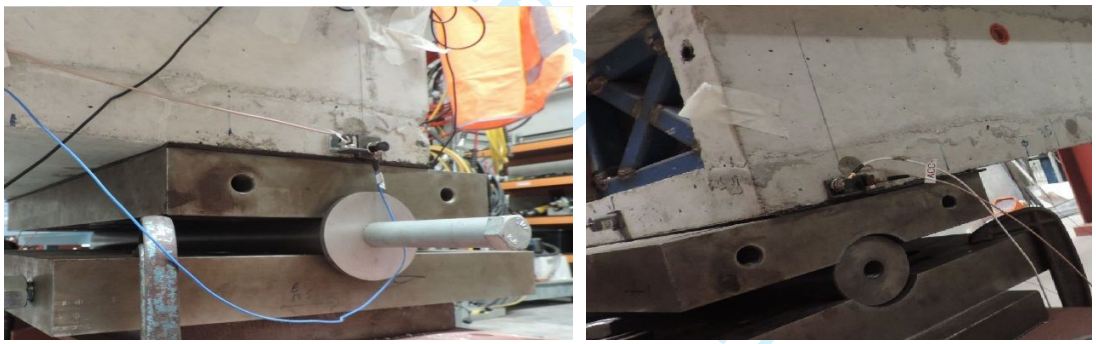

(b)

Figure 1. The BGB details: (a) BGB's dimensions and (b) Boundary conditions in BGB as Roller (left) and Pin (right).

In the second state (damaged state), a point load and then a cyclic load were applied at the midspan of the BGB. These impacts resulted in some significant cracks on

the soffit slab and the webs of the BGB. Eight significant cracks were observed, each of which ran through the whole width of the bottom slab and propagated to the webs. Figure 2 shows some observed cracks on the body of the structure.

Figure 2. Detected cracks on body of the BGB in damaged state.

Numerical model

Given the lack of available information about the structural parameters of the BGB, such as material properties and boundary conditions, nominal values of the parameters were assumed from the designing details and were used to create a numerical model of the BGB. The initial BGB's FEM was built in the Abaqus software package, as shown in Figure 3 (Abaqus, 2017).

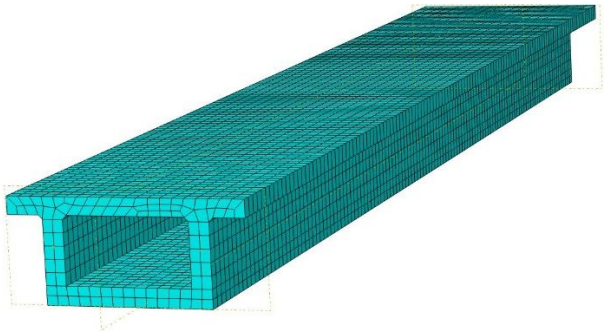

Figure 3. FEM of BGB built in ABAQUS 2017.

From the Abaqus element library, a C3D8R solid element and a T3D2 truss element were assigned to the concrete and reinforcement elements, respectively. Regarding material properties, according to the design details, Young's modulus (E) is assumed as 200 (GPa) for reinforcement and 32 (GPa) for concrete. Further, mass density (ρ) is assumed as 7,850 kg/m^3 for reinforcement and 2,400 kg/m^3 for concrete. In addition, the boundary conditions were considered fixed in vertical displacement for both supports. In this study, a convergence assessment for mesh size selection was performed by applying a load-displacement control. Herein, load against midspan deflection was examined for different mesh sizes. A mesh size of 50 mm was determined to be fit enough by considering the experimental displacement at the mid-zone in failure mode. More details of the analysis can be found in Jamali et al. (2018). In this study, four natural frequencies of the FEM—first vertical bending, second vertical bending, first lateral bending, and third vertical bending modes—were selected

and used to update the FEM because similar mode shapes and natural frequencies were extracted from the measured data.

Modal data analysis

During the casting process of the BGB, several small steel plates were attached to the BGB's surface to facilitate sensor installation. The sensory system used in this study is shown in Figure 4 (a). Regarding the selection of the right sensor layout, different aspects were noticed in relation to the number and type of available sensors, the excitation source, and the maximum number of channels in the data acquisition system. More details regarding the preparation of the experiment can be found in Jamali et al. (2016). The BGB was excited by applying multipoint random excitation with an impact hammer for each vibration test. Vibration responses were recorded using a data acquisition system. In this study, the vibration responses of the structure in both the undamaged and damaged states were measured and used in the FEMU process. Figure 4 (b) shows three examples of sensor layout arrangements that were applied in the modal analysis in this research. Each arrow in the figure represents a single sensor in the corresponding direction.

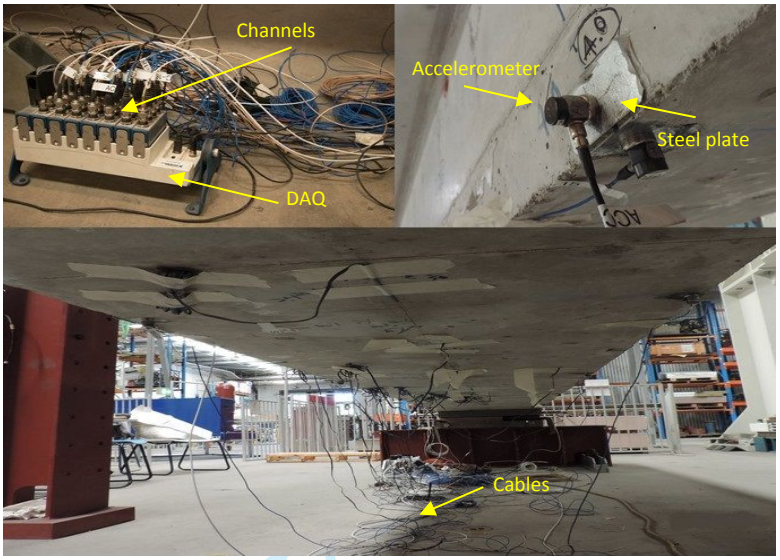

(a)

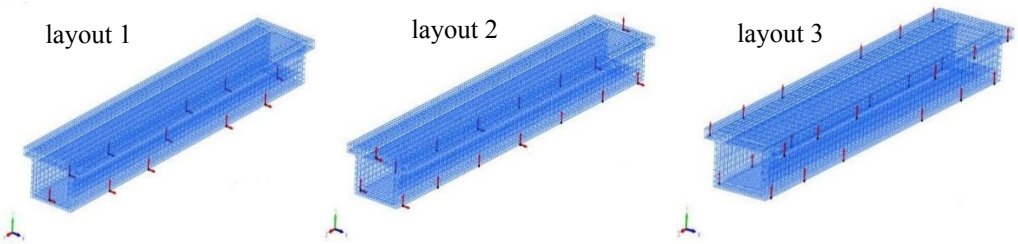

(b)

Figure 4. Structural response measurement: (a) Sensory system on the BGB and (b) Sensor layouts.

The measured acceleration responses were post-processed in the modal analysis step. In this regard, the stochastic subspace identification (SSI) method, which is embedded in the ARTeMIS Modal software package, was applied (ARTeMIS, 2011). An example of modal analysis for a dataset is illustrated in Figure 5.

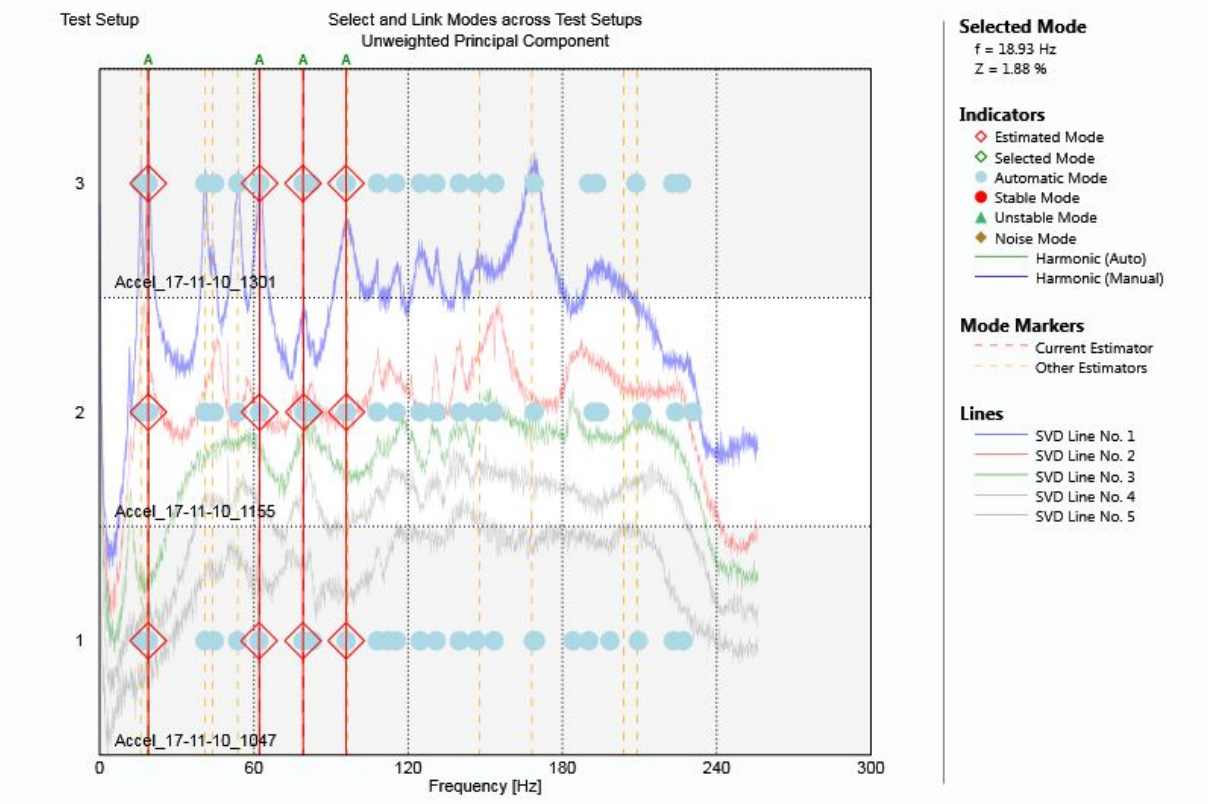

Figure 5. Modal Analysis to capture experimental frequency in ARTeMIS.

Modal parameters for 40 datasets in the undamaged state and 60 datasets in the damaged state were analyzed. The test was conducted in a controlled environment in the laboratory, where ambient effects had little effect on the measured responses; therefore, the number of modal analyses in both states was sufficient. The detected natural frequencies were the first vertical bending, second vertical bending, first

lateral bending, and third vertical bending modes, similar to the FEM's results. These modes were selected for the FEMU process because they could be detected in both the undamaged and damaged states. The four measured mode shapes were transferred into the FEMtools software package (Dynamic Design Solutions, 2012). The number of degrees of freedom (DOF) of an experimental model is often smaller than that of the corresponding FEM as a result of a lack of available sensors (Moravej et al., 2017). In this study, a coordinate expansion technique was applied to increase the number of DOFs of the experimental model to the same number in the FEM (Moravej et al., 2017). The values of the natural frequencies in both states are shown in Table 1. In this table, the mode order refers to the ordering number of the modes. The experimental and numerical mode shapes are illustrated in Figure 6.

Table 1. Frequency in the initial designed model and measured frequency in two states

Mode order	Freq as Designed (Hz)	Measured Freq (Undamaged)		Error (%)	Measured Freq (Damaged)		Error (%)
		Mean value (Hz)	STD		Mean value (Hz)	STD	
1	24.339	21.65	0.106	-12.42	18.78	0.082	-29.60
2	81.29	67.06	0.21	-21.22	63.06	0.174	-28.9
3	92.108	84.32	0.124	-9.24	80.73	0.14	-14.09
4	109.75	98.21	0.18	-11.75	95.74	1.023	-14.63

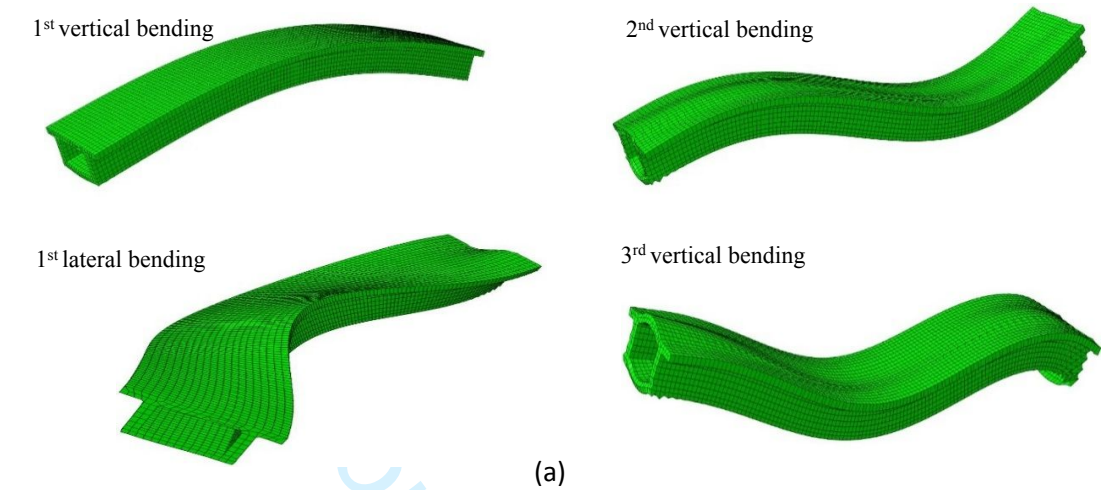

(a)

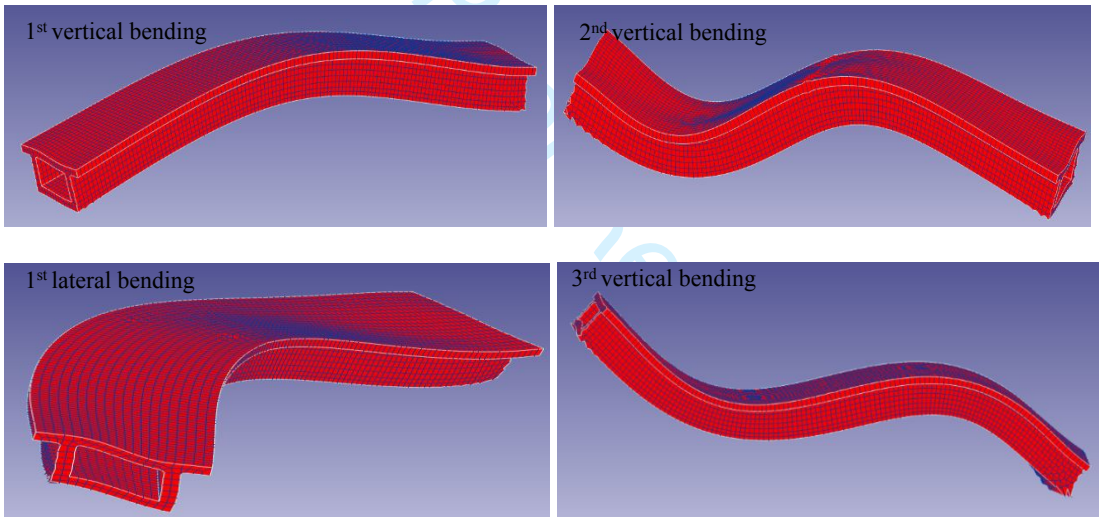

(b)

Figure 6. Four mode shapes: (a) Numerical model and (b) Measured model.

Sensitivity analysis

A key step in most model updating approaches is the selection of appropriate parameters and responses in advance to initiate the updating process. Sensitivity analysis is a technique used to select the most sensitive parameters to the responses of a numerical model. This technique tends to analyse the effect of a very small perturbation of a parameter's value on a response by sketching the tangents on the response-parameter curve (Mottershead and Friswell, 2011). In this study, differential sensitivity analysis was applied to choose the most sensitive parameters to the selected responses using FEMtools (Dynamic Design Solutions, 2012). A differential sensitivity coefficient was calculated as the slope of the response T_i in relation to parameter B_j at a known state of the parameter. Once these differentials were calculated for all selected responses in relation to all selected parameters, sensitivity matrix **S** was generated by equation (11).

$$\mathbf{S} = S_{ij} = \frac{\delta T_i}{\delta B_j} \tag{11}$$

where:

i: 1,...,n *T:* Responses

j: 1,...,n *B:* Parameters

Each column of the sensitivity matrix corresponds with a parameter B_j and each row corresponds with a response T_i. Regarding the responses in this experiment, the four modal frequencies identified in the previous subsections were selected as sensitive responses. Details of the selected responses are shown in Table 1.

In the initial FEM, the simple supports were modelled as fixed in the vertical direction. However, by applying a correlation analysis between the mode shapes from the FEM and those from the experiment, it was observed that the roller in the experimental model was not fixed, as a bouncing was observed in the second vertical mode shape, as shown in Figure 7. Further, similar results were obtained for the third vertical bending mode shape. Therefore, a more accurate simulation of the boundary condition was used in this study to better represent the behavior of the structure.

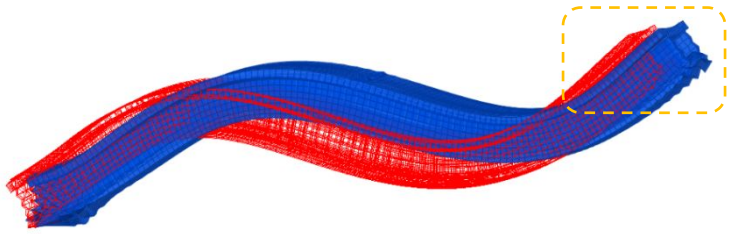

Figure 7. Correlation between FEM (Blue) and experimental (Red) in 2nd vertical mode shape.

For the updating process, the parameters related to concrete in three different parts (i.e., bottom slab, webs, and top slab) were selected separately because the BGB was cast in the three corresponding steps. Further, observed changes in the health condition of the three parts were different after the damage was induced. Hence, the parameter selection resulted in 10 parameters: (1) Young's modulus of concrete (top), (2) Young's modulus of concrete (web), (3) Young's modulus of concrete (bottom), (4) Young's modulus of reinforcement, (5) vertical spring stiffness (roller), (6) vertical spring stiffness (pinned), (7) mass density of reinforcement, (8) mass density of concrete (top), (9) mass density of concrete (web), and (10) mass density of concrete (bottom). Results of the sensitivity analysis, as shown in Figure 8, provide a clearer picture of which parameters were sensitive to the selected responses. The vertical axis in this figure refers to sensitivity magnitude. Based on the sensitivity analysis, the selection resulted in the five most sensitive parameters: Young's moduli of the bottom slab, the webs, and the top slab (E_{cBot}, E_{cWeb}, and E_{ctop}); and vertical spring stiffness coefficients of the two supports (K_{roller} and K_{pin}). Reducing the number of parameters of interest is essential to decrease the computational cost.

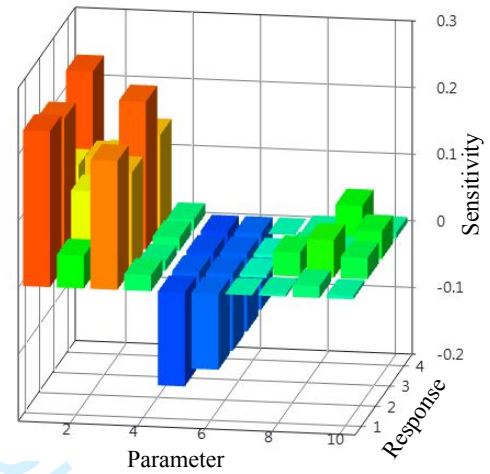

Figure 8. Sensitivity Analysis between selected parameters and responses.

Result and discussion

The FEM of the BGB was updated for the two states—undamaged and damaged—by applying the MBA and using the four natural frequencies, mentioned in the previous section, as the responses. This section highlights the outcomes regarding the calibrated parameters and predicted responses in both states.

FEMU for undamaged state

There was a lack of testing results from the casting stage, such as core sampling and tensile strength, to provide insights into prior distribution. Therefore, normal distributions were selected to represent all parameters' prior probability distribution

functions. This was in line with Mirza et al. (1980), Darmawan and Stewart (2007) and recommendations from the code of practice AS-5104, as shown in Table 2.

Table 2. Parameter Prior Probability Distribution in Undamaged state

Parameter	Mean	Coefficient of Variation
(E_{cTop}) Young's modulus - Concrete - Top slab	32 GPa	7.13
(E_{cWeb}) Young's modulus - Concrete - Web	32 GPa	7.13
(E_{cBot}) Young's modulus - Concrete - Bottom slab	32 GPa	7.13
(K_{Roller}) Spring Stiffness Roller support	5×10^{7} N/m	9×10^{13}
(K_{Pin}) Spring Stiffness Pinned support	5×10^{7} N/m	9×10^{13}

In this study, the computational process was carried out using a computer equipped with an Intel i7 quad-core processor with 3.4 GHz speed, 16 GB of RAM, and a fast-access solid-state drive (SSD). For modules 1 and 2, hyperparameters were obtained that characterize the estimation of the calibrated parameters and the discrepancy function, and consequently represent the GPs. These hyperparameters included a variance matrix $\sum$, a matrix of regression coefficient β, roughness parameters ω, and a noise variance matrix Λ, as explained in the methodology. Results of the calibrated parameters after applying the MBA in the undamaged state are illustrated in Figure 9 and Table 3. The posterior may require more data before it faithfully represents the calibrated parameters; as a result, it did not present any

changes compared with the prior. It is worth noting that the likelihood identified the calibrated parameters according to the measured data. As shown in Figure 9, in the undamaged state, there were no considerable changes in Young's moduli of the webs and the top slab in the likelihood against their priors. A significant change was observed in the reduction in the bottom slab's Young's modulus (E_{cBot}), which was identical to the observed minor cracks beneath the BGB. Another noticeable change was a reduction in vertical spring stiffness at the roller support, which infers that the vertical fixity at the roller support was overestimated. This outcome is well matched with the observed bouncing in the roller previously noticed in Figure 7.

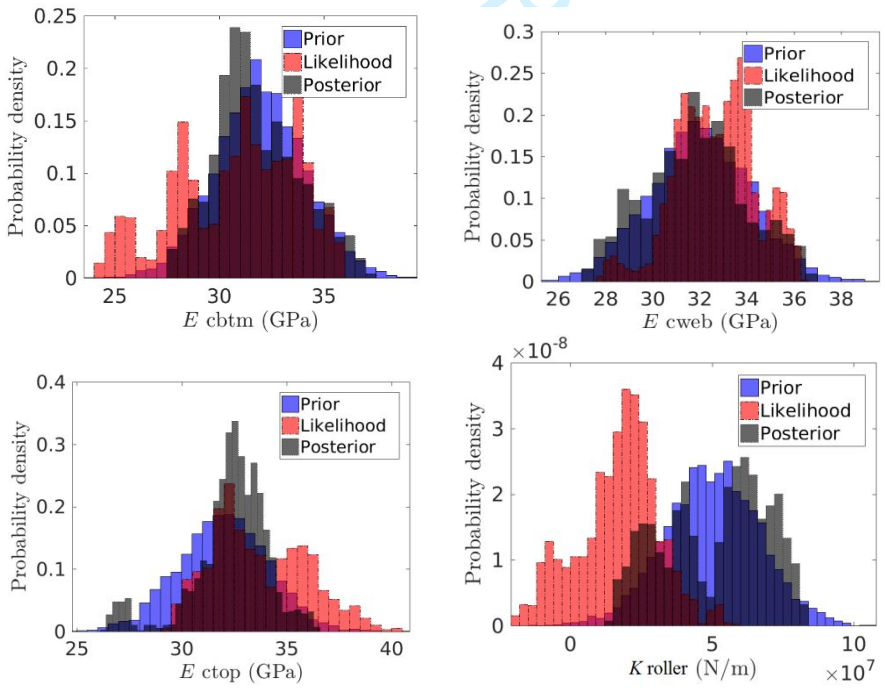

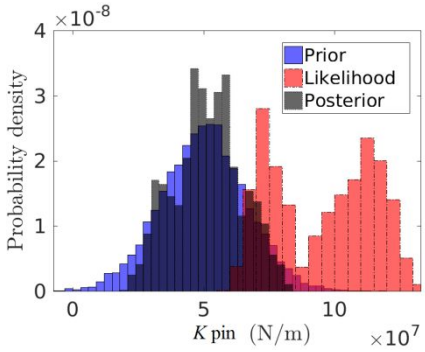

Figure 9. Prior, Max Likelihood and Posterior PDF for calibrated parameters in undamaged state.

Table 3. The Likelihood and Posterior distribution for calibrated parameters in undamaged state

	Posterior		Likelihood	
Part	Mean	Coefficient of Variation	Mean	Coefficient of Variation
E_{cBot}	31.81 (GPa)	4.1	30.84 (GPa)	8.3
E_{cWeb}	31.83 (GPa)	4.5	32.69 (GPa)	2.9
E_{cTop}	32.34 (GPa)	3.4	33.67 (GPa)	5.2
K_{Roller}	5.10×10^{7} (N/m)	3.32×10^{14}	1.68×10^{7} (N/m)	2.02×10^{14}
K_{Pin}	5.15×10^{7} (N/m)	1.66×10^{14}	9.53×10^{7} (N/m)	3.82×10^{14}

The discrepancy functions for all four modes in the undamaged state are depicted in Figure 10 (a). In this figure, the horizontal axis represents the sample ordering numbers of the simulated data. The black line represents the predicted mean, and

the shaded region denotes a 95% prediction interval. As shown, the MBA predicted the measured responses accurately for all modes, with deviations of less than 6%.

Figure 10 (b) depicts the measured responses together with the prediction intervals for all four modal frequencies. The measured data points obtained from the experimental tests, as shown by red spots in Figure 10 (b), are randomly distributed among the simulated data points. As shown, the measured data points are located in the 95% prediction interval and are very close to the mean values of the predicted responses. The predicted mean values almost coincide with those of the measured data points for all modes (see Table 1). However, it can be inferred from the predictions that the higher the mode order that is examined, the larger the scatter interval that is obtained.

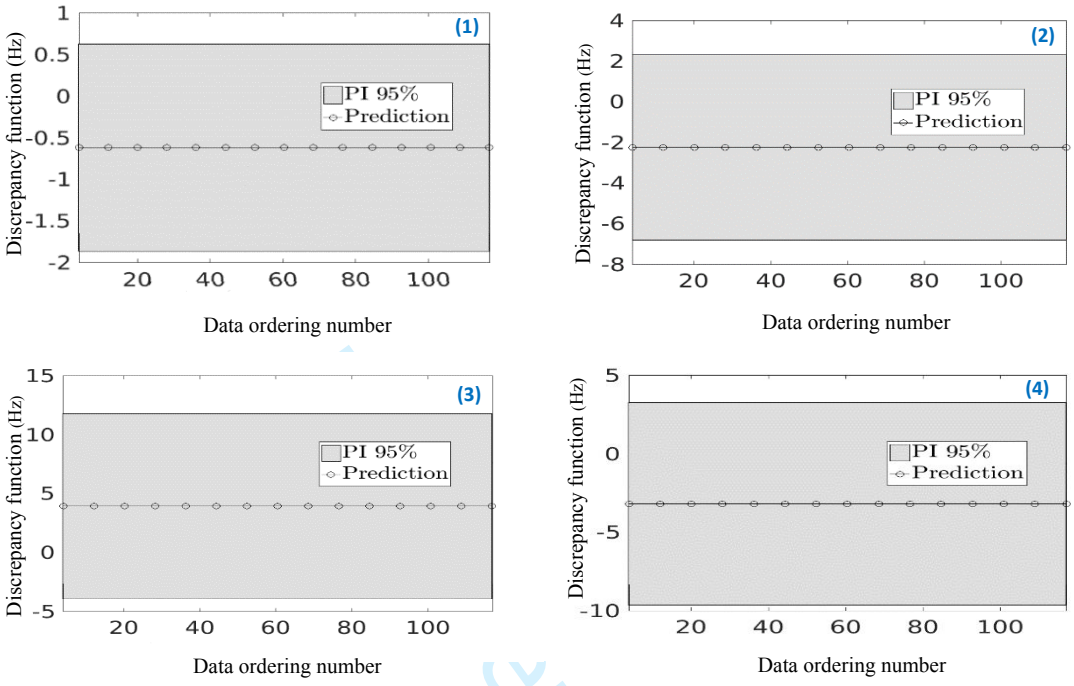

(a) Discrepancy functions for frequency responses.

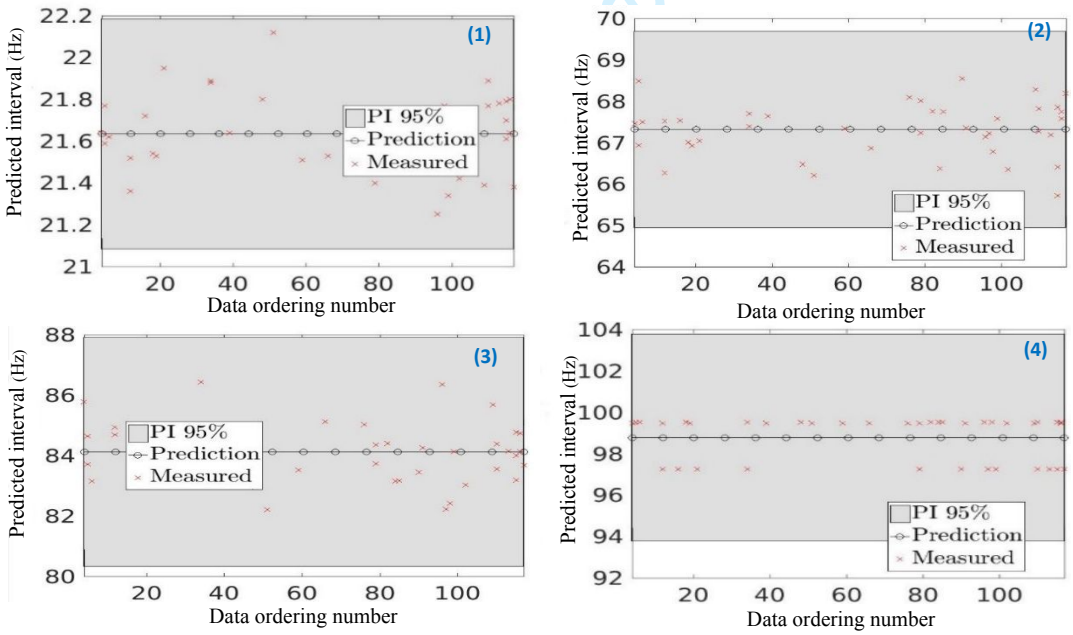

(b) Predicted interval 95% confidence for numerical model and experimental data points.

Figure 10. The results of Discrepancy function and predicted response for numerical model in undamaged state for all four modal frequencies as: (1) 1st vertical bending frequency, (2) 2nd vertical bending frequency, (3) 1st lateral bending frequency & (4) 3rd vertical bending frequency.

FEMU for damaged state

The next step of model updating refers to the damaged state, where some significant cracks were observed on the bottom slab and the webs of the BGB. It is worth mentioning that the number of calibrated parameters was reduced to three (Young's moduli) because it was assumed that the applying impacts in the damaged state did not affect the boundary conditions. Results of the prior, likelihood, and posterior distributions of the calibrated parameters are illustrated in Figure 11 and Table 4.

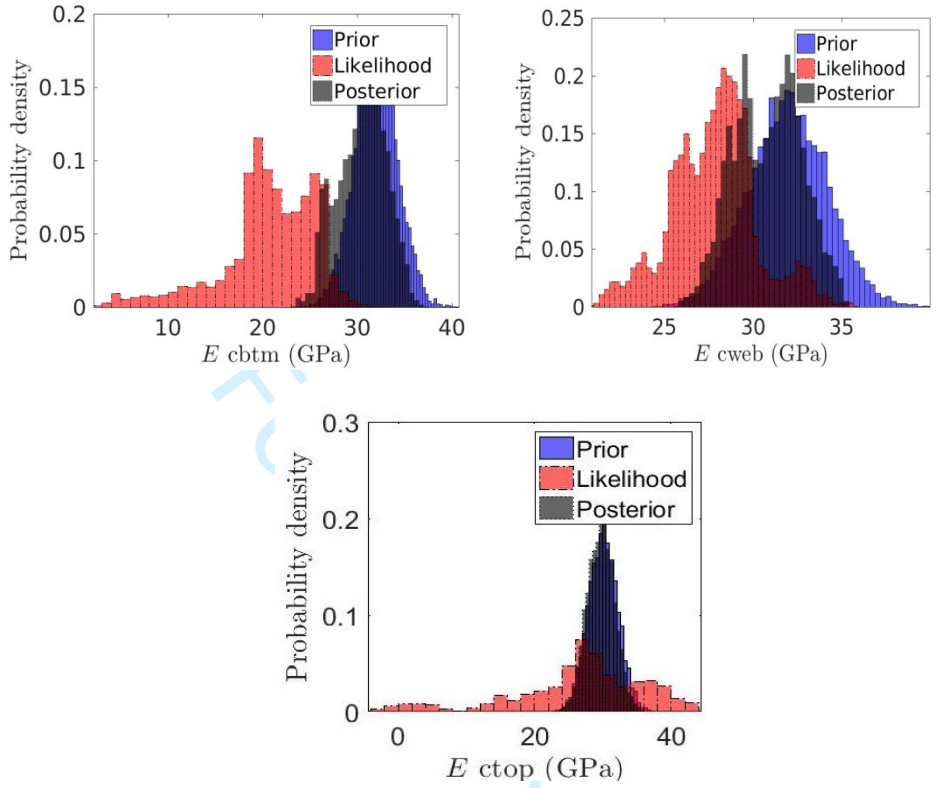

Figure 11. Prior, Max Likelihood and Posterior PDF for calibrated parameters in damaged state.

Table 4. The Likelihood and Posterior distribution for calibrated parameters in damaged state

	Posterior		Likelihood	
Part	mean	Coefficient of Variation	mean	Coefficient of Variation
E_{cBot}	30.45 (GPa)	6.45	20.63 (GPa)	25.59
E_{cWeb}	30.82 (GPa)	3.58	27.82 (GPa)	5.99
E_{cTop}	32.54 (GPa)	2.26	30.54 (GPa)	35.45

As shown in Figure 11, a significant change was targeted at the likelihood in Young's modulus of the bottom slab, indicating a reduction of about 35.5% to a new mean value of 20.63 GPa. Further, the decrease in Young's modulus of the web section was noticeable, showing a likelihood mean of 27 GPa. The impact forces had little effect on the top slab, and its updated Young's modulus was almost the same as its initial value. The reduction in the Young's moduli of the bottom slab and the webs is well matched with the cracks observed in the damaged state, as mentioned in the section *Two states of box girder bridge*. The discrepancy functions for all four modes in the damaged state are depicted in Figure 12 (a). As shown in the figure, the discrepancy increases in the damaged state, especially for the second and third vertical bending modes. In addition, the discrepancy functions in the damaged state are distributed more sparsely than those in the undamaged state. This may be because the cracks cause nonlinearities in the properties of structural materials and the mechanism of the experimental response.

Results of the measured responses together with predicted intervals for all four modes are shown in Figure 12 (b). As shown, the measured data points are observed in the corresponding predicted intervals and are very close to the mean values for all modes except the last one (third vertical bending mode). Results for the third vertical bending mode are very scattered. It is worth noting that the discrepancy of this mode is larger than that of the other modes, as shown in Figure 12 (b). This can

be explained because nonlinearity effects resulting from cracks become more significant when the vibration mode contains a higher-order curve.

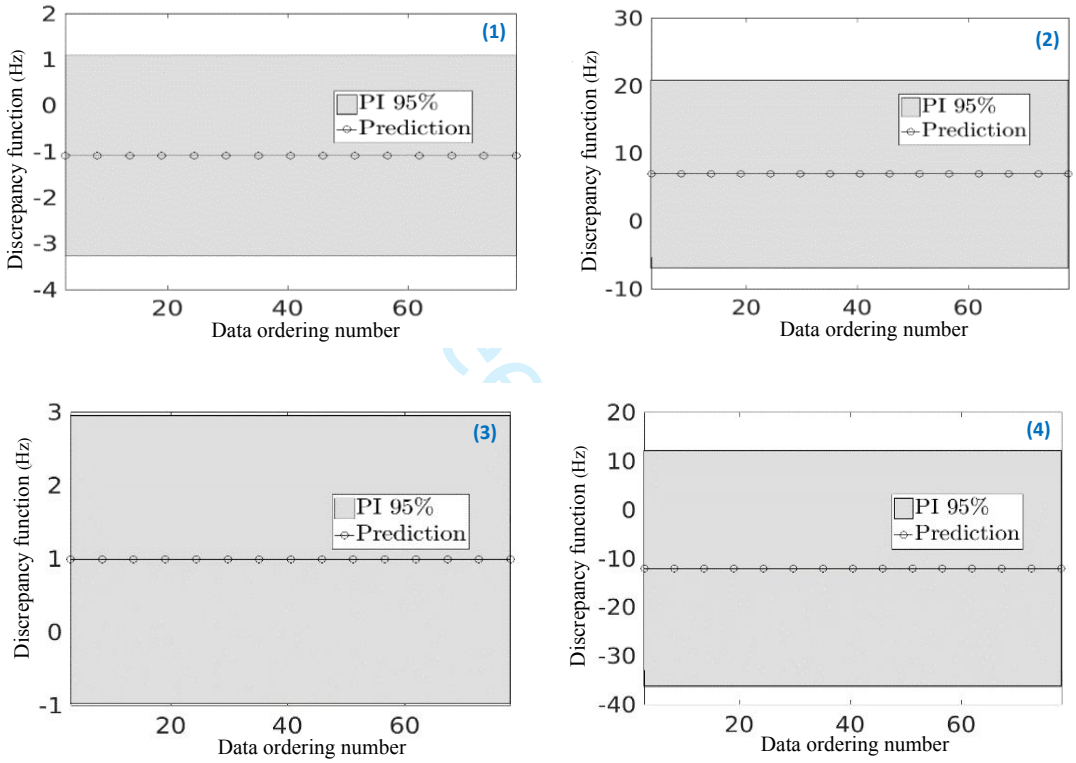

(a) Discrepancy functions for frequency responses.

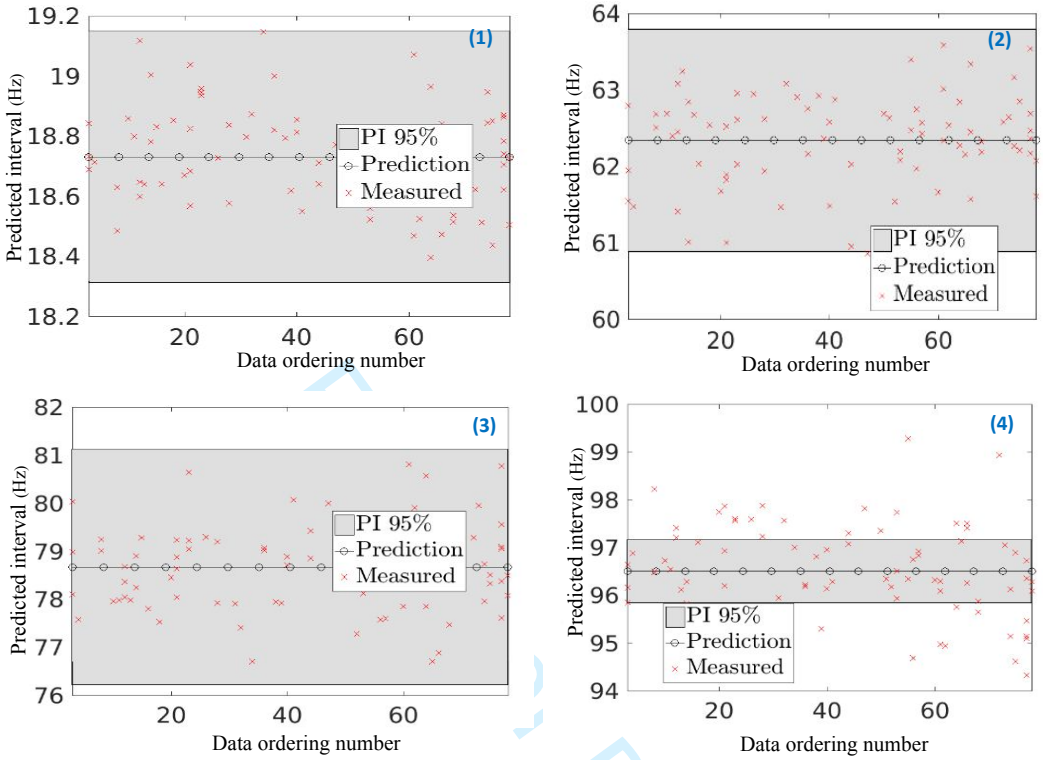

(b) Predicted interval 95% confidence for numerical model and experimental data points.

Figure 12. The results of discrepancy function and predicted response for numerical model in damaged state, for all four modal frequencies as: (1) 1st vertical bending frequency, (2) 2nd vertical bending frequency, (3) 1st lateral bending frequency & (4) 3rd vertical bending frequency.

Conclusions

In this study, the performance of an MBA was investigated in a large lab-scaled BGB using vibration data. Sensitivity analysis was conducted to select the most sensitive parameters and responses. Further, a metamodel was used instead of a

whole numerical model. Therefore, the computational task and processing time was reduced in comparison with other probabilistic updating techniques. This benefit distinguishes this approach, especially in applications to complex structures.

This study is the first to apply the MBA for two different states: damaged and undamaged. These two states represent the health conditions of the structure during its life span, and the outcomes can be used for further structural investigations. Although a case study is rather simple compared with full-scale real structures, such a scale provides a possibility to investigate the performance of the proposed approach in two different states according to the observed evidence on the structure. Further, this study highlighted the advantages of FEMU because it illustrated that even an FEM of a downscaled structure requires accurate calibration to be reliably used in further structural assessments.

Moreover, in contrast to many previous studies, which applied the MBA to a single parameter, this study investigated model updating on multiple parameters, such as material properties and boundary conditions, at the same time. In this study, the changes to these parameters were well matched with the observed evidence in both states. Natural frequencies of the first four modes, used as the measured data points, were predicted correctly. The updated model was sufficiently matched with the physical observation of the damaged structure. In turn, the results generated from

this study might be attributed to the proposed uncertainty quantification methodology. Further, as the results showed in the damaged state, the discrepancy functions increased, and experimental responses were not predicted as accurately as in the undamaged state. Such increases in the discrepancy functions are inferred as a guide for designers, implying that the FEM needs to be refined by considering additional aspects such as crack modeling. Further, response prediction can be improved and discrepancy can be reduced by adding other experimental data points (e.g., strain and mode shape) and information about environmental conditions (e.g., temperature and humidity). Although natural frequency was selected as the response for the updating process in this study, the MBA is capable of considering other types of responses. Thus, the performance of the approach when applied to other responses, such as mode shape, should be investigated in future studies. Consequently, the proposed methodology contributes to more reliable judgments about structural safety and more informed maintenance decision-making.

Acknowledgments

The first author would like to express his sincere appreciation to Queensland University of Technology (QUT) for the financial support for his research. The support provided by Australian Research Council (ARC) via a Discovery Project (DP160101764) is also gratefully acknowledged. Also, the support provided by technical support from FEMtools is acknowledged.

References

Arendt, P.D., Apley, D.W. and Chen, W (2012a) Quantification of model uncertainty: Calibration, model discrepancy, and identifiability. *Journal of Mechanical Design* 134(10):100908-100908-12.

Arendt, P.D., Apley, D.W., Chen, W., Lamb, D. and Gorsich, D (2012b) Improving identifiability in model calibration using multiple responses. *Journal of Mechanical Design* 134(10) 100909-100909-9.

Abaqus, F.E.A. (2017) Abaqus Inc. *Providence, Rhode Island, United States*.

Bayarri, M. J., Berger, J. O., Paulo, R., Sacks, J., Cafeo, J. A., Cavendish, J., Lin, C. H., and Tu, J (2007) "A Framework for Validation of Computer Models," *Technometrics* 49(2), pp. 138–154.

Beck, J.L. and Au, S.K. (2002) Bayesian updating of structural models and reliability using Markov chain Monte Carlo simulation. *Journal of engineering mechanics* 128(4), pp.380-391.

Beck, J.L. and Katafygiotis, L. S (1998) Updating models and their uncertainties. I: Bayesian statistical framework. *Journal of Engineering Mechanics* 124(4), pp.455-461.

Conde, B., Eguía, P., Stavroulakis, G.E. and Granada, E. (2018) Parameter identification for damaged condition investigation on masonry arch bridges using a Bayesian approach. *Engineering Structures* 172, pp.275-284.

Conti, S., Gosling, J.P., Oakley, J.E. and O'Hagan, A. (2009) Gaussian process emulation of dynamic computer codes. *Biometrika* 96(3), pp.663-676.

Darmawan, M.S. and Stewart, M.G. (2007) Spatial time-dependent reliability analysis of corroding pretensioned prestressed concrete bridge girders. *Structural Safety* 29(1), pp.16-31.

FEMtools UM (2012) *FEMtools Dynamic Design Solutions* N.V. (DDS)

Frangopol, D.M. (2011) Life-cycle performance, management, and optimisation of structural systems under uncertainty: accomplishments and challenges 1. *Structure and Infrastructure Engineering* 7(6), pp.389-413.

Friswell, M. and Mottershead, J.E. (2013) Finite element model updating in structural dynamics (Vol. 38). Springer Science & Business Media.

General principles on reliability for structures (AS 5104)

Higdon, D., Gattiker, J., Williams, B. and Rightley, M. (2008) Computer model calibration using high-dimensional output. *Journal of the American Statistical Association* 103(482), pp.570-583.

Jamali, S., Chan, T.H., Nguyen, A. and Thambiratnam, D.P. (2018) Reliability-based load-carrying capacity assessment of bridges using structural health monitoring and nonlinear analysis. *Structural Health Monitoring* 18(1), pp. 20–34.

Jamali, S., Chan, T.H., Thambiratnam, D.P., Pritchard, R. and Nguyen, A. (2016) Pre-test finite element modelling of box girder overpass-application for bridge condition assessment. In *Australasian Structural Engineering Conference: ASEC 2016* (p. 457). Engineers Australia.

Jesus, A., Brommer, P., Westgate, R., Koo, K., Brownjohn, J. and Laory, I. (2018) Bayesian structural identification of a long suspension bridge considering temperature and traffic load effects. *Structural Health Monitoring*
https //doi.org/10.1177/1475921718794299

Jesus, A., Brommer, P., Westgate, R., Koo, K., Brownjohn, J., & Laory, I. (2019) Modular Bayesian damage detection for complex civil infrastructure. *Journal of Civil Structural Health Monitoring* 1-15.

Jesus, A., Brommer, P., Zhu, Y. and Laory, I. (2017) Comprehensive Bayesian structural identification using temperature variation. *Engineering Structures* 141, pp.75-82.

Jesus, A.H., Dimitrovová, Z. and Silva, M.A. (2014) A statistical analysis of the dynamic response of a railway viaduct. *Engineering Structures* 71, pp.244-259.

Kennedy, M. and O'Hagan, A. (2001a) Bayesian calibration of computer models. *Journal of the Royal Statistical Society: Series B (Statistical Methodology)* 63(3), pp.425-464.

Kennedy, M. and O'Hagan, A. (2001b). Supplementary details on Bayesian calibration of computer. Rap. tech., University of Nottingham *Statistics Section*.

Li, H.N., Li, D.S., Ren, L., Yi, T.H., Jia, Z.G. and Li, K.P. (2016) Structural health monitoring of innovative civil engineering structures in Mainland China. *Structural Monitoring and Maintenance* 3(1), pp.1-32.

Liu, F., Bayarri, M.J. and Berger, J.O. (2009) Modularization in Bayesian analysis, with emphasis on analysis of computer models. *Bayesian Analysis* 4(1), pp.119-150.

Lophaven, S.N., Nielsen, H.B. and Søndergaard, J. (2002) *DACE: a Matlab kriging toolbox* (Vol. 2). IMM, *Informatics and Mathematical Modelling, the Technical University of Denmark.*

Mirza, S.A., Kikuchi, D.K. and MacGregor, J.G. (1980) Flexural strength reduction factor for bonded prestressed concrete beams. In *Journal Proceedings* (Vol. 77, No. 4, pp. 237-246).

Moravej H, Jamali S, Chan THT, Nguyen A. (2017) Finite element model updating of civil engineering infrastructures: a review literature. *International Conference on Structural Health Monitoring of Intelligent Infrastructure. Brisbane, Australia 2017.*

Mottershead, J.E., Link, M. and Friswell, M.I. (2011) The sensitivity method in finite element model updating: a tutorial. *Mechanical systems and signal processing* 25(7), pp.2275-2296.

O'Hagan, A. (2006) Bayesian analysis of computer code outputs: A tutorial. *Reliability Engineering & System Safety* 91(10-11), pp.1290-1300.

Pathirage TS. (2017). Identification of prestress force in prestressed concrete box girder bridges using vibration-based techniques. *Queensland University of Technology.*

Rasmussen, C. and Williams, C. (2006) Gaussian Processes for Machine Learning. *Adaptive Computation and Machine Learning.*

Shahidi, S.G. and Pakzad, S.N. (2013) Generalized response surface model updating using time domain data. *Journal of Structural Engineering* 140(8), p.A4014001.

Simoen, E., Papadimitriou, C. and Lombaert, G. (2013) On prediction error correlation in Bayesian model updating. *Journal of Sound and Vibration* 332(18), pp.4136-4152

Structural Vibration Solutions A/S (2011) SVS-ARTeMIS Extractor-Release 5.3, User's manual. Aalborg-Denmark

Weng, S., Xia, Y., Zhou, X.Q., Xu, Y.L. and Zhu, H.P. (2012) Inverse substructure method for model updating of structures. *Journal of Sound and Vibration* 331(25), pp.5449-5468.

Vibration-based Bayesian model updating of civil engineering structures applying Gaussian process metamodel

Hossein Moravej, Tommy Chan, Khac-Duy Nguyen and

Andre Jesus

Abstract

Structural health monitoring plays a significant role in providing information regarding the performance of structures throughout their life spans. However, information that is directly extracted from monitored data is usually susceptible to uncertainties and not reliable enough to be used for structural investigations. Finite element model updating (FEMU) is an accredited framework that reliably identifies structural behavior. Recently, the modular Bayesian approach (MBA) has emerged as a probabilistic technique in calibrating the finite element model (FEM) of structures and comprehensively addressing uncertainties. However, few studies have investigated its performance on real structures. In this paper, MBA is applied to calibrate the FEM of a lab-scaled concrete box girder bridge. This

study is the first to use the MBA to update the initial FEM of a real structure for two states—undamaged and damaged conditions—in which the damaged state represents changes in structural parameters as a result of aging or overloading. The application of the MBA in the two states provides an opportunity to examine the performance of the approach with observed evidence. A discrepancy function is used to identify the deviation between the outputs of the experimental and numerical models. To alleviate computational burden, the numerical model and the model discrepancy function are replaced by Gaussian processes. Results indicate a significant reduction in the stiffness of concrete in the damaged state, which is identical to cracks observed on the body of the structure. The discrepancy function reaches satisfying ranges in both states, which implies that the properties of the structure are predicted accurately. Consequently, the proposed methodology contributes to a more reliable judgment about structural safety.

Keywords

Finite Element Model Updating, Bayesian framework, Gaussian process, Structural Health Monitoring, Box girder bridge, Vibration analysis

Introduction

Civil infrastructure plays a significant role in keeping urban systems operational, but any malfunctions in routine performance can result in major hazards and even threaten lives. Therefore, it is important to regularly investigate the safety of infrastructure. Many researchers such as Frangopol (2011) and Li et al. (2016) have acknowledged the importance of monitoring the behaviors of structures using information provided by structural health monitoring (SHM). An accredited approach to addressing the aforementioned objective is finite element model updating (FEMU), which aims to improve the accuracy of the finite element models (FEMs) of real structures and reduce the discrepancy between the output of FEMs and experimental measurements. The availability of reliable FEMs of structures is beneficial in terms of evaluation of structural performance, reliability analysis, load-carrying capacity assessment, and damage detection.

However, FEMU faces significant barriers that prevent it from reaching its peak efficiency. For example, computational burden, especially in the case of complex structures, makes this technique cumbersome, and in some cases, the process of updating may lead to ill-conditioned optimization problems with limited practical applicability. Although some approaches have recently been introduced to improve computational efficiency, such as the response surface method (Shahidi and Pakzad,

2013) and the substructure technique (Weng et al., 2012), this challenge still needs to be addressed.

Another challenge when updating a model relates to addressing different sources of uncertainties. To overcome this problem, probabilistic approaches that are more reliable than their deterministic counterparts have been introduced in the field of FEMU (Jesus et al., 2014; Jesus et al., 2018). Deterministic techniques, which consider fixed values regarding input parameters and response outputs, rarely provide a satisfactory correlation between the numerical model and real data because of inherent structural uncertainties (Friswell and Mottershead, 2013). In contrast, probabilistic approaches do not regard input parameters as fixed numbers to lock the updating process in those values; instead, they consider a realistic statistical distribution for each parameter. This consideration is more logical because it is impossible to confidently assert a certain value for one parameter using an updating process because of the existence of uncertainties. Therefore, in most cases, probabilistic approaches are more reliable. According to Kennedy and O'Hagan (2001a, 2001b), the main sources of uncertainty in model prediction are uncertainty in model parameters, modeling errors, and uncertainty resulting from observation errors. Uncertainty in model parameters relates to inputs to the computer model that are unknown and cannot be identified directly from physical experiments, such as the material properties of a damaged structure. Another source

of uncertainty—modeling error or model inadequacy—refers to any assumptions or simplifications made while developing FEMs, such as considering a material linear, isotropic, and homogenous. This source of uncertainty occurs even when all parameters are accurately identified. The observation error (i.e., experimental uncertainty) is usually present in physical experiments. This type of uncertainty denotes variations that may occur in the experimental measurement even when the test is repeated with the same settings.

Despite the significant effects of the abovementioned uncertainties, few studies have addressed all of these aspects. A number of probabilistic approaches have been developed in FEMU, including the fuzzy number-based method, Kalman Filter-based technique, model falsification diagnosis method, Markov process-based method and sampling method. Among all probabilistic FEMU techniques, Bayesian updating has been found to be one of the most applicable approaches for updating FEMs. Several attempts have been made to apply Bayesian updating, and Beck's method is eminent among them because it proposes a robust predictive approach (Beck and Katafygiotis, 1998; Beck and Au, 2002). The major weakness in the presentation of Bayesian methods in SHM practices is that uncertainty resulting from modeling errors is not properly considered. Only a few researchers have performed the Bayesian approach with consideration of this aspect (Higdon et al., 2008; Simoen et al., 2013). Higdon used a comprehensive modular Bayesian

approach (MBA) that was formerly established by Kennedy and O'Hagan (2001a), but it was not generally successful in addressing identifiability. Identifiability represents the ability to achieve the true value of model parameters based on available data to illustrate a physical property such as Young's modulus (Arendt et al., 2012a). Arendt et al. (2012b) proposed an improvement to Kennedy and O'Hagan's original formulation using the MBA to overcome the identifiability problem by applying measured data with various responses. This method replaces an FEM with a Gaussian process (GP) model as a metamodel (Kennedy and O'Hagan, 2001a). It has been found that the method significantly reduces computational effort—especially in cases of complex structures (Lophaven et al., 2002; Jesus et al., 2017; Conde et al., 2019; Jesus et al., 2019). The GP model for interpolation that considers uncertainties is found to be effective, even if data are limited. This formulation is preferable to former studies in model updating because it comprises the main sources of uncertainties and consequently reaches more realistic outcomes.

Based on the thriving interest in the MBA, this study validates its practical performance in FEMU by means of measured vibration data. The study investigates the applicability of the algorithm to a lab-scaled reinforced concrete box girder bridge (BGB), which represents a typical hollow core bridge deck in Australia. The MBA is applied in two states—undamaged and damaged—to calibrate multiple

parameters of the FEM. The performance of the approach is examined according to the observed evidence of the undamaged condition with initial minor cracks and the damaged condition with imposed cracks. The damaged state represents changes in structural parameters as a result of aging or overloading. Accordingly, this study aims to identify changes in the structural parameters and provide a reliable updated model for each state. The structural identification provided through the applied framework will not only provide a better understanding of structural performance, but will also contribute to providing suitable guidelines for decision-making regarding maintenance actions.

Model Updating Methodology

This section describes the model updating approach used in this study. The first subsection explains the connecting equation between the observations and the outputs of the numerical model. The second subsection briefly presents the GP, and the last subsection outlines the framework.

Observation and numerical model relationship

We assume that a real and unobservable process f has n observations of q responses $\mathbf{Y^e}$ from the measured data, where the superscript "**e**" is the experimental model. The relationship between $\boldsymbol{f}$ and $\mathbf{Y^e}$ can be denoted as equation (1):

$$\mathbf{Y^e} = \boldsymbol{f} + \varepsilon \quad \textbf{(}1\text{)}$$

where $\varepsilon = [\varepsilon_1, \ldots, \varepsilon_n]^T$ is the observation error, which is supposed to work as a Gaussian distribution with a mean of 0 and variance of $\Lambda \in \mathbb{R}$. Alternatively, the real process f can be interpreted as equation (2) to comprise the numerical model:

$$\boldsymbol{f} = \mathbf{Y}^m(\theta^*) + \boldsymbol{\delta} \quad (2)$$

where $\boldsymbol{\delta}$ is a discrepancy function that represents the difference between the numerical model and the real process. $\mathbf{Y}^m(\theta^*)$ is the numerical model's output and θ^* is an r-dimensional vector of the true structural parameters. This equation is an idealized form of the final model (i.e., the model after successful calibration), while the model parameters θ take the values θ^*. Significantly, the discrepancy function

does not depend on the model's output and is an unknown in addition to the structural parameters. Equation (2) is then substituted into equation (1) to obtain equation (3):

$$\mathbf{Y^e} = \mathbf{Y^m}(\theta^*)+\boldsymbol{\delta}+\varepsilon \quad (3)$$

Equation (3) is a comprehensive equation of the model updating process. It denotes the output of the processes within the domain of a calibrated status $\theta = \theta^*$, which implies the best fit compared with the observed data.

In the next step, the numerical model and the discrepancy function are substituted with two multiple-response Gaussian processes (MRGPs) whose hyperparameters must be found. These hyperparameters describe the MRGPs and illustrate the approximation of their associated uncertainties such as variability of the numerical model, modeling discrepancies, and observation errors.

Gaussian Process

Gaussian processes (GP) modeling is an interpolation approach that considers uncertainty highly efficient even when data are limited (Kennedy and O'Hagan, 2001a; Rasmussen et al., 2006). By applying interpolations and extrapolations, this

approach offers a predicted GP that is fitted on all observation points. In this study, an MRGP is applied by assuming that the metamodel of model **Y** is a single realization of a spatial random process with a prior mean function and covariance function (O'Hagan, 2006; Rasmussen et al., 2006). Regarding approximation of the metamodel, it is assumed that a dataset of **Y** with a size of g and N observations should be available as input. Dimension g represents the number of responses (Y_1, Y_2,..., Y_g). To generate the MRGP, the mean function is required to be obtained, which exists at every design input point without uncertainty. In the spaces located between or outside the design input points, the MRGP will produce either a possible interpolation or extrapolation from the existing data points.

In the MRGP, the prior mean function is supposed to be a member of a hierarchical structure of linear functions. It can be generalized as the form $\mathbf{M}=\mathbf{H}\boldsymbol{\beta}$. Herein, matrix **H** comprises N polynomial constant regression functions and the matrix of regression coefficient $\boldsymbol{\beta}$ for each term included in matrix **H** and each fitted response in **Y**. That is, **H** is a row vector of regression functions and $\boldsymbol{\beta}$ is a column vector of regression functions.

The prior covariance function of the MRGP for the model and discrepancy function can be formulated as equation (4):

$$\mathbf{V} = \sum^2 \otimes \mathbf{R} \quad (4)$$

where $\mathbf{V}$ is covariance function, $\sum^{\mathbf{2}} \in \mathbb{R}^{g \times g}$ is a non-temporal variance matrix, and $\mathbf{R} \in \mathbb{R}^{N \times N}$ is a temporal correlation matrix, and $\otimes$ is the Kronecker product operation on the two matrices. This equation can be interpreted as the separation of a variance between the *g* responses (which are being approximated) and a correlation between the *N* times histories. Each entry of Matrix **R** contains a correlation function that needs to be approximated. This assumption is applicable to the correlation function of the numerical model. In addition, because the FEM is linear, a linear correlation function is assumed for the correlation function in this study, as shown in equation (5). This model fits properly to the data and is numerically stable (Lophaven et al., 2002).

$$\mathbf{R}(\omega, \theta, \theta') = \prod_{j=1}^{r} \max\{0, 1 - \omega_j |\theta_j - \theta'_j|\} \quad (5)$$

In equation (5), ω_j ($j=1,...,r$) is the roughness parameter and represents how roughly the responses change from point θ to point θ' for each of the structural parameters of interest.

In contrast, the correlation matrix for the discrepancy function is simply assumed as an identity matrix as **R**=**I**. This assumption implies that the final predicted

responses have no temporal correlation. This is reasonable for natural frequencies obtained from a laboratory model because they vary randomly without any definite relations. The final hyperparameter that needs to be estimated to conclude the description of the MRGP is Λ as the $N\times1$ variance vector of the observation error ε, which can simply be added to equation (4) to reach equation (6).

$$\mathbf{V} = \sum^2 \otimes \mathbf{R} + \Lambda \tag{6}$$

After providing a certain amount of data $\mathbf{Y}$, the MRGP is provided (supposing a non-informative prior for $\boldsymbol{\beta}$ and given ω and $\sum$). The posterior distribution of the response is given by equation (7):

$$y \mid \boldsymbol{\Sigma}, \omega, \Lambda, \mathbf{Y} \sim N(m^*, \boldsymbol{\Sigma} \otimes \gamma^*) \tag{7}$$

with

$$m^* = h\hat{\boldsymbol{\beta}} + \boldsymbol{\gamma}^{\mathbf{T}} \boldsymbol{\Gamma}^{-1} (\mathbf{Y} - \mathbf{H}\hat{\boldsymbol{\beta}}) \tag{8}$$

$$\gamma^* = \gamma - \boldsymbol{\gamma}^{\mathbf{T}} \boldsymbol{\Gamma}^{-1} \gamma + [h^T - \mathbf{H}^{\mathbf{T}} \boldsymbol{\Gamma}^{-1} \gamma]^T [\mathbf{H}^{\mathbf{T}} \boldsymbol{\Gamma}^{-1} \mathbf{H}]^{-1} [h^T - \mathbf{H}^{\mathbf{T}} \boldsymbol{\Gamma}^{-1} \gamma] \tag{9}$$

where y represents the MRGP, *h* is the hierarchical structure of regression functions. $\boldsymbol{\gamma}$ is defined as a relational correlation matrix, which maps the correlation between the indices of points of available dataset and the indices of points supposed to be predicted (Conti et al., 2009). The used correlation function is the same as equation (5). $\hat{\boldsymbol{\beta}}$ stands for the estimated matrix of $\boldsymbol{\beta}$ and is given by calculating equation (10):

$$\mathbf{H}^{\mathbf{T}}\mathbf{R}^{-1}\mathbf{H}\hat{\boldsymbol{\beta}} = \mathbf{H}^{\mathbf{T}}\mathbf{R}^{-1}\mathbf{Y} \tag{10}$$

which refers to the linear regression solution of the best linear unbiased predictor. $\boldsymbol{\Gamma}$ is an $N \times N$ correlation matrix that contains the linear functions. The MRGP in equation (7) can be defined by estimating the hyperparameters ω, $\boldsymbol{\beta}$, $\sum$, and Λ. Characterization of the hyperparameters can be conducted using a Bayesian approach, which would address all of the mentioned uncertainties and identify all of the hyperparameters at the same time. However, this approach is not efficient because it comprises a huge computational process (Liu et al., 2009). Therefore, for better computational efficiency, the hyperparameters are calculated with the maximum likelihood estimations (MLEs). A more comprehensive description of the GP method can be found in Arendt et al. (2012a).

Modular Bayesian approach (MBA)

The MBA separates the updating process into four steps. The hyperparameters of the MRGP are approximated separately and consecutively, as shown in Figure 5 in the study by Arendt et al. (2012a). In the MBA, the hyperparameters continue to be estimated until the first order of uncertainties is found, and then they are fixed. It is worth noting that setting up the hyperparameters at fixed estimations decreases the degree of approximation of the uncertainties. In addition, the "second-order" resolution of the uncertainties is ignored to alleviate the computational burden and make it faster than fully considering the uncertainties in the Bayesian framework. This act of estimating and fixing the hyperparameters is performed sequentially when progressing from module 1 to module 2 and from module 2 to module 3.

The first module basically substitutes the computer model to an MRGP model and estimates its hyperparameters based on only the simulation data. In this module, the simulation is run in finite element modeling software (e.g., Abaqus) to obtain the simulated responses by randomly changing the input parameters using Latin hypercube sampling (LHS). For the experimental validation in this study, 120 and 80 runs were conducted in the undamaged and damaged states, respectively, to provide a dataset. The estimation can be carried out using numerical optimization methods by fitting a likelihood between the MRGP and the available simulation

data. In this study, a genetic algorithm (GA) routine was applied in MATLAB. For the GA setup, an initial population of size 40 is generated in the [0; 1] range, a Gaussian mutation function with a scale of 1 (i.e., initial standard deviation of 1) and a standard deviation shrink of 1 is chosen, and a scattered crossover function applied to a portion of 0.8 of the population at each generation is defined. Convergence criteria are set as either a maximum number of 100 generations or until an average change in the fitness value of 1×10^{-6} is reached.

In module 2, the discrepancy function is estimated by fitting another MRGP model according to the measured data from the experiment, the simulation data, and the prior distribution of the calibration parameters. The GA is used to approximate the discrepancy function by estimating the hyperparameters of the GP. This task is carried out by an MLE, which indicates that the fitness function of the GA is a likelihood function. It should be mentioned that either the MBA or the full Bayesian approach can estimate the hyperparameters of the abovementioned MRGP models through MLE and Bayesian posterior distributions, respectively. As discussed in the previous section, the MBA is used in this study because Bayesian posterior distributions can be computationally inefficient. In addition, according to Bayarri et al. (2007), both approaches have similar results in predicting the discrepancy function and calibration parameters.

In module 3, Bayes' theorem is applied to approximate the posterior distribution of the updated parameters and its likelihood function containing the two MRGP models approximated in modules 1 and 2. Since multiple parameters are calibrated in this study, a Markov chain Monte Carlo method can be used to estimate the MBA. This choice implies that a target distribution must be used, and in this study, a multivariate normal distribution is chosen (Arendt et al., 2012b).

In module 4, the experimental responses are calculated by applying the measured data and the estimated hyperparameters obtained from modules 1 and 2. After the simulated and measured data are collected in modules 1 and 2 and the calibrated parameters are estimated in module 3, the posterior distribution response of the updated model together with the updated discrepancy function can be obtained. For the prediction of the responses, 40 measured data points for the undamaged state and 60 data points for the damaged state are randomly distributed along the simulated data points. It is worth noting that simulated data have been provided by applying the LHS approach as described in the first module. In addition, it is assumed that the measured responses are independent of time, temperature variation, and other operational effects.

Finite element model updating for a box girder bridge

The first subsection presents details of the BGB and two different states (i.e., undamaged and damaged) of the structure. Details of an FEM and experimental modal analysis as two counterparts in model updating are provided in the second and third subsections, respectively. The fourth subsection highlights sensitivity analysis as a tool to select appropriate parameters and responses in FEMU.

Two states of box girder bridge

A downscaled reinforced concrete BGB, which was constructed in the civil engineering laboratory at the Queensland University of Technology, is investigated in this study. This structure represents a typical in-service hollow core bridge deck in Australia. The length of the BGB is 6 m, and it was cast in three separate parts as the bottom slab, the webs, and the top slab. Detailed dimensions of the structure are shown in Figure 1 (a). Further information about the casting steps can be found in Pathirage (2017). The BGB was placed on two simple supports as a pin at one end and a roller at the other end, as shown in Figure 1 (b). This platform refers to the undamaged state (first state), despite the existence of some minor cracks beneath the soffit slab.

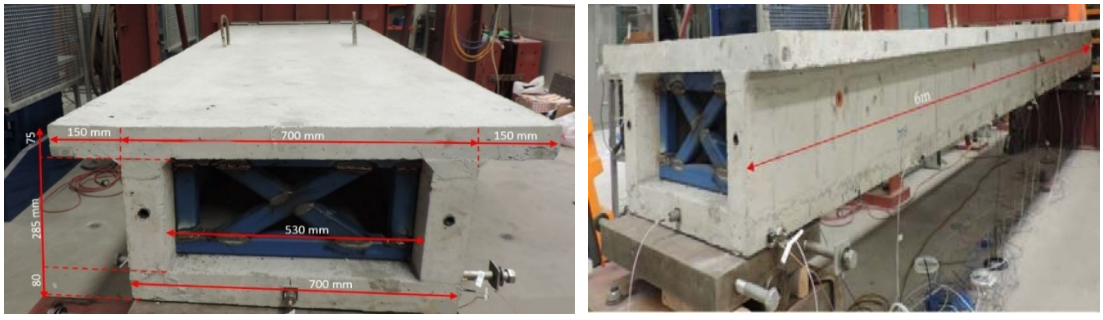

(a)

(b)

Figure 1. The BGB details: (a) BGB's dimensions and (b) Boundary conditions in BGB as Roller (left) and Pin (right).

In the second state (damaged state), a point load and then a cyclic load were applied at the midspan of the BGB. These impacts resulted in some significant cracks on the soffit slab and the webs of the BGB. Eight significant cracks were observed, each of which ran through the whole width of the bottom slab and propagated to the webs. Figure 2 shows some observed cracks on the body of the structure.

Figure 2. Detected cracks on body of the BGB in damaged state.

Numerical model

Given the lack of available information about the structural parameters of the BGB, such as material properties and boundary conditions, nominal values of the parameters were assumed from the designing details and were used to create a numerical model of the BGB. The initial BGB's FEM was built in the Abaqus software package, as shown in Figure 3 (Abaqus, 2017).

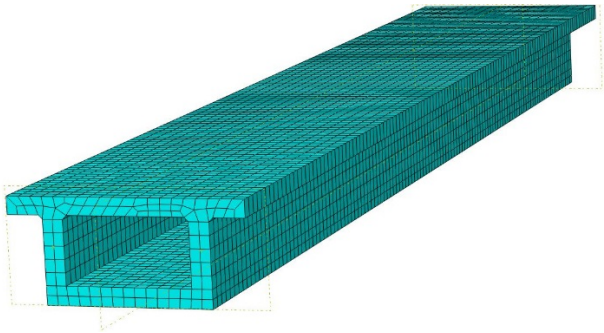

Figure 3. FEM of BGB built in ABAQUS 2017.

From the Abaqus element library, a C3D8R solid element and a T3D2 truss element were assigned to the concrete and reinforcement elements, respectively. Regarding material properties, according to the design details, Young's modulus (E) is assumed as 200 (GPa) for reinforcement and 32 (GPa) for concrete. Further, mass density (ρ) is assumed as 7,850 kg/m^3 for reinforcement and 2,400 kg/m^3 for concrete. In addition, the boundary conditions were considered fixed in vertical displacement for both supports. In this study, a convergence assessment for mesh size selection was performed by applying a load-displacement control. Herein, load against midspan deflection was examined for different mesh sizes. A mesh size of 50 mm was determined to be fit enough by considering the experimental displacement at the mid-zone in failure mode. More details of the analysis can be found in Jamali et al. (2018). In this study, four natural frequencies of the FEM—first vertical bending, second vertical bending, first lateral bending, and third vertical bending modes—were selected

and used to update the FEM because similar mode shapes and natural frequencies were extracted from the measured data.

Modal data analysis

During the casting process of the BGB, several small steel plates were attached to the BGB's surface to facilitate sensor installation. The sensory system used in this study is shown in Figure 4 (a). Regarding the selection of the right sensor layout, different aspects were noticed in relation to the number and type of available sensors, the excitation source, and the maximum number of channels in the data acquisition system. More details regarding the preparation of the experiment can be found in Jamali et al. (2016). The BGB was excited by applying multipoint random excitation with an impact hammer for each vibration test. Vibration responses were recorded using a data acquisition system. In this study, the vibration responses of the structure in both the undamaged and damaged states were measured and used in the FEMU process. Figure 4 (b) shows three examples of sensor layout arrangements that were applied in the modal analysis in this research. Each arrow in the figure represents a single sensor in the corresponding direction.

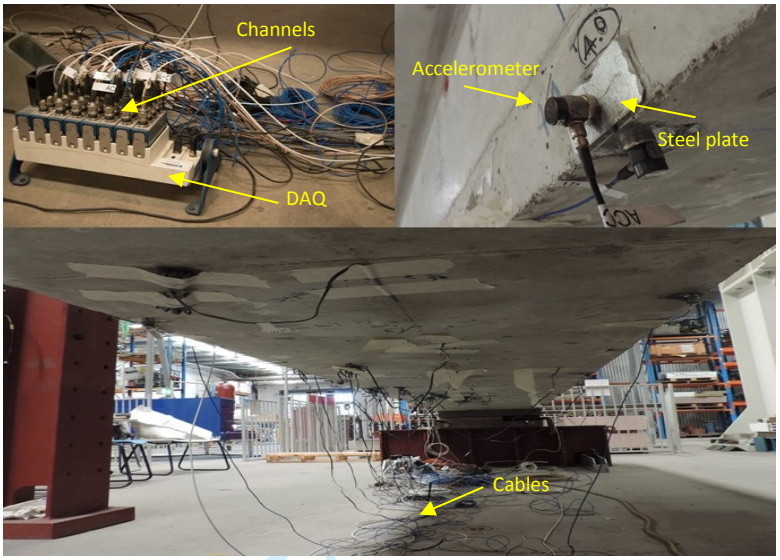

(a)

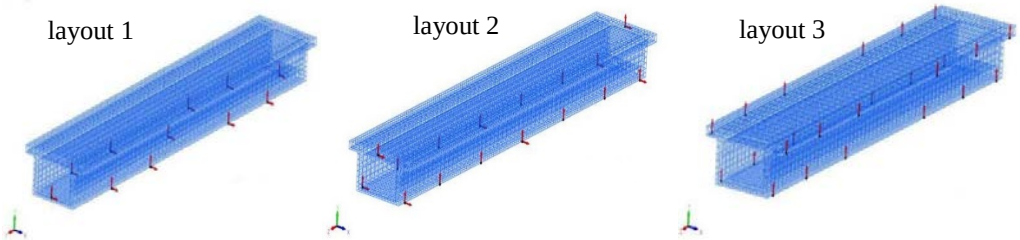

(b)

Figure 4. Structural response measurement: (a) Sensory system on the BGB and (b) Sensor layouts.

The measured acceleration responses were post-processed in the modal analysis step. In this regard, the stochastic subspace identification (SSI) method, which is embedded in the ARTeMIS Modal software package, was applied (ARTeMIS, 2011). An example of modal analysis for a dataset is illustrated in Figure 5.

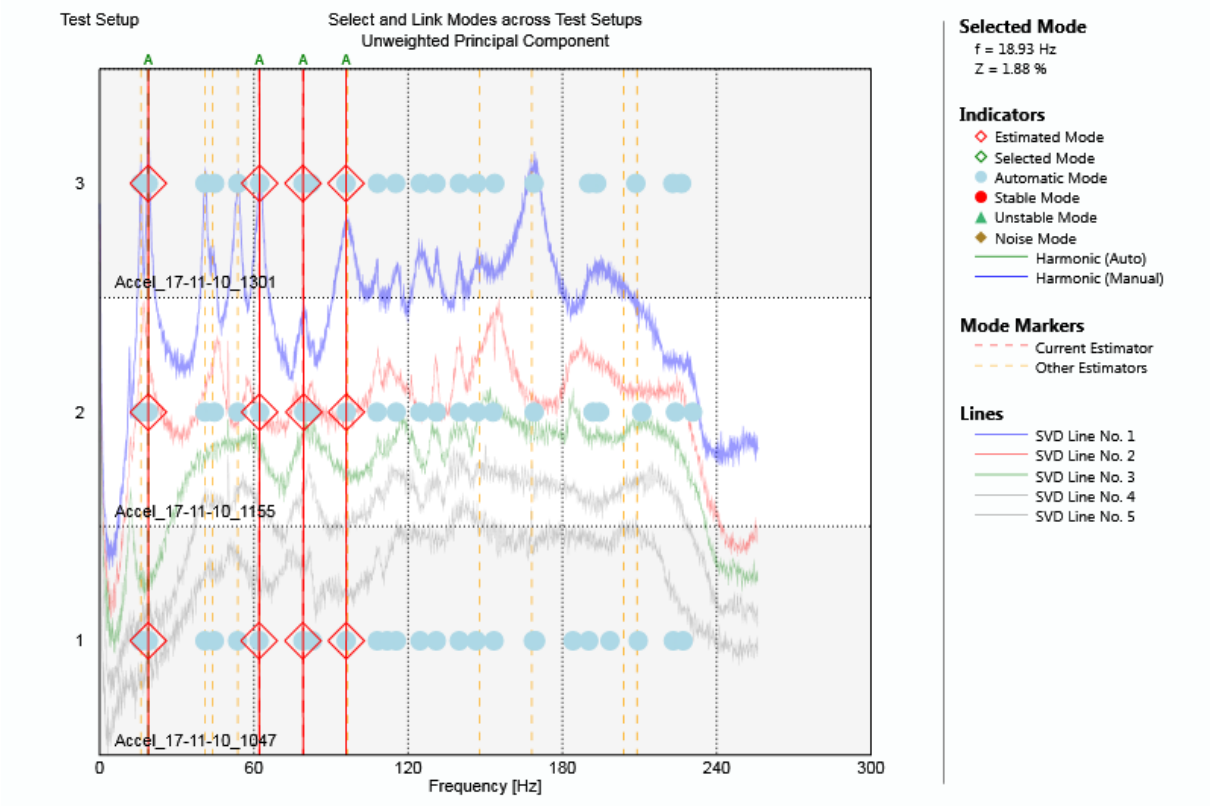

Figure 5. Modal Analysis to capture experimental frequency in ARTeMIS.

Modal parameters for 40 datasets in the undamaged state and 60 datasets in the damaged state were analyzed. The test was conducted in a controlled environment in the laboratory, where ambient effects had little effect on the measured responses; therefore, the number of modal analyses in both states was sufficient. The detected natural frequencies were the first vertical bending, second vertical bending, first

lateral bending, and third vertical bending modes, similar to the FEM's results. These modes were selected for the FEMU process because they could be detected in both the undamaged and damaged states. The four measured mode shapes were transferred into the FEMtools software package (Dynamic Design Solutions, 2012). The number of degrees of freedom (DOF) of an experimental model is often smaller than that of the corresponding FEM as a result of a lack of available sensors (Moravej et al., 2017). In this study, a coordinate expansion technique was applied to increase the number of DOFs of the experimental model to the same number in the FEM (Moravej et al., 2017). The values of the natural frequencies in both states are shown in Table 1. In this table, the mode order refers to the ordering number of the modes. The experimental and numerical mode shapes are illustrated in Figure 6.

Table 1. Frequency in the initial designed model and measured frequency in two states

Mode order	Freq as Designed (Hz)	Measured Freq (Undamaged)		Error (%)	Measured Freq (Damaged)		Error (%)
		Mean value (Hz)	STD		Mean value (Hz)	STD	
1	24.339	21.65	0.106	-12.42	18.78	0.082	-29.60
2	81.29	67.06	0.21	-21.22	63.06	0.174	-28.9
3	92.108	84.32	0.124	-9.24	80.73	0.14	-14.09
4	109.75	98.21	0.18	-11.75	95.74	1.023	-14.63

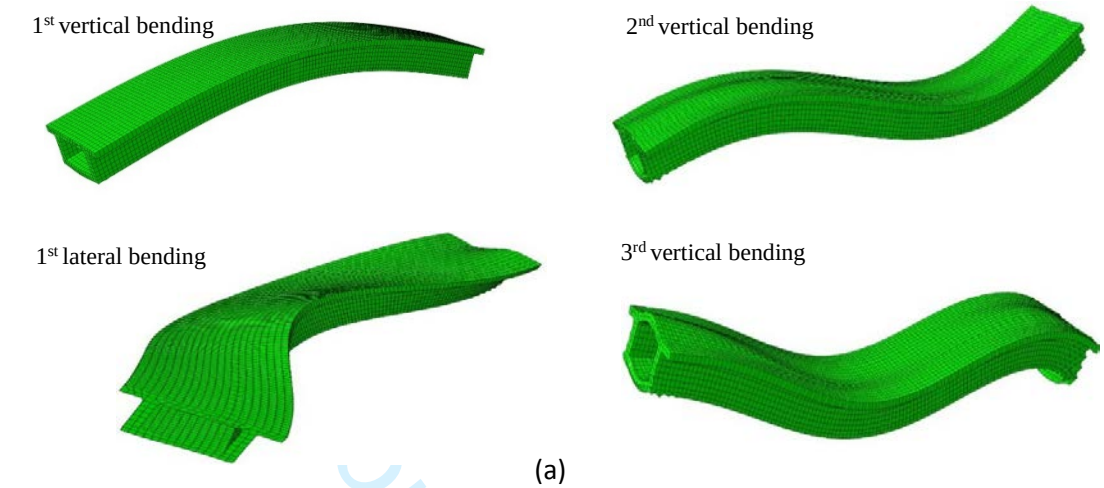

(a)

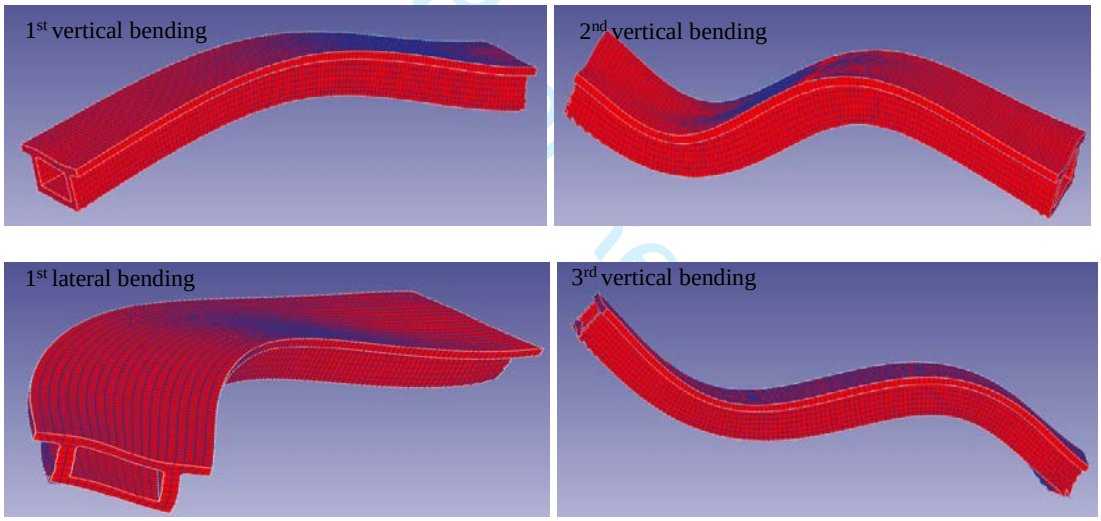

(b)

Figure 6. Four mode shapes: (a) Numerical model and (b) Measured model.

Sensitivity analysis

A key step in most model updating approaches is the selection of appropriate parameters and responses in advance to initiate the updating process. Sensitivity analysis is a technique used to select the most sensitive parameters to the responses of a numerical model. This technique tends to analyse the effect of a very small perturbation of a parameter's value on a response by sketching the tangents on the response-parameter curve (Mottershead and Friswell, 2011). In this study, differential sensitivity analysis was applied to choose the most sensitive parameters to the selected responses using FEMtools (Dynamic Design Solutions, 2012). A differential sensitivity coefficient was calculated as the slope of the response T_i in relation to parameter B_j at a known state of the parameter. Once these differentials were calculated for all selected responses in relation to all selected parameters, sensitivity matrix **S** was generated by equation (11).

$$\mathbf{S} = S_{ij} = \frac{\delta T_i}{\delta B_j} \tag{11}$$

where:

i: 1,…,n *T:* Responses

j: 1,…,n *B:* Parameters

Each column of the sensitivity matrix corresponds with a parameter B_j and each row corresponds with a response T_i. Regarding the responses in this experiment, the four modal frequencies identified in the previous subsections were selected as sensitive responses. Details of the selected responses are shown in Table 1.

In the initial FEM, the simple supports were modelled as fixed in the vertical direction. However, by applying a correlation analysis between the mode shapes from the FEM and those from the experiment, it was observed that the roller in the experimental model was not fixed, as a bouncing was observed in the second vertical mode shape, as shown in Figure 7. Further, similar results were obtained for the third vertical bending mode shape. Therefore, a more accurate simulation of the boundary condition was used in this study to better represent the behavior of the structure.

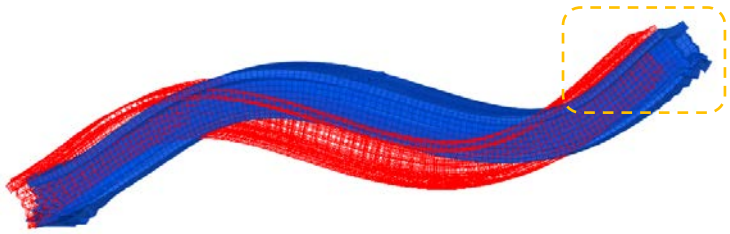

Figure 7. Correlation between FEM (Blue) and experimental (Red) in 2nd vertical mode shape.

For the updating process, the parameters related to concrete in three different parts (i.e., bottom slab, webs, and top slab) were selected separately because the BGB was cast in the three corresponding steps. Further, observed changes in the health condition of the three parts were different after the damage was induced. Hence, the parameter selection resulted in 10 parameters: (1) Young's modulus of concrete (top), (2) Young's modulus of concrete (web), (3) Young's modulus of concrete (bottom), (4) Young's modulus of reinforcement, (5) vertical spring stiffness (roller), (6) vertical spring stiffness (pinned), (7) mass density of reinforcement, (8) mass density of concrete (top), (9) mass density of concrete (web), and (10) mass density of concrete (bottom). Results of the sensitivity analysis, as shown in Figure 8, provide a clearer picture of which parameters were sensitive to the selected responses. The vertical axis in this figure refers to sensitivity magnitude. Based on the sensitivity analysis, the selection resulted in the five most sensitive parameters: Young's moduli of the bottom slab, the webs, and the top slab (E_{cBot}, E_{cWeb}, and E_{ctop}); and vertical spring stiffness coefficients of the two supports (K_{roller} and K_{pin}). Reducing the number of parameters of interest is essential to decrease the computational cost.

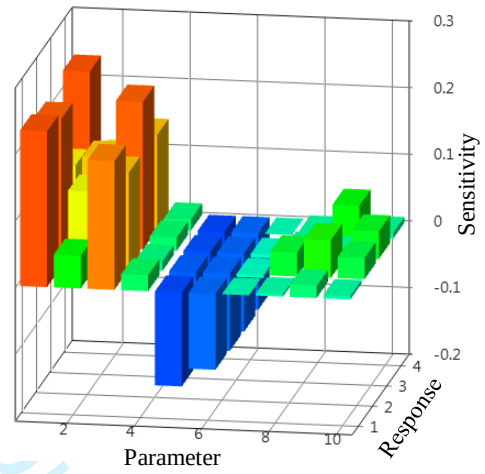

Figure 8. Sensitivity Analysis between selected parameters and responses.

Result and discussion

The FEM of the BGB was updated for the two states—undamaged and damaged—by applying the MBA and using the four natural frequencies, mentioned in the previous section, as the responses. This section highlights the outcomes regarding the calibrated parameters and predicted responses in both states.

FEMU for undamaged state

There was a lack of testing results from the casting stage, such as core sampling and tensile strength, to provide insights into prior distribution. Therefore, normal distributions were selected to represent all parameters' prior probability distribution

functions. This was in line with Mirza et al. (1980), Darmawan and Stewart (2007) and recommendations from the code of practice AS-5104, as shown in Table 2.

Table 2. Parameter Prior Probability Distribution in Undamaged state

Parameter	Mean	Coefficient of Variation
(E_{cTop}) Young's modulus - Concrete - Top slab	32 GPa	7.13
(E_{cWeb}) Young's modulus - Concrete - Web	32 GPa	7.13
(E_{cBot}) Young's modulus - Concrete - Bottom slab	32 GPa	7.13
(K_{Roller}) Spring Stiffness Roller support	5×10^{7} N/m	9×10^{13}
(K_{Pin}) Spring Stiffness Pinned support	5×10^{7} N/m	9×10^{13}

In this study, the computational process was carried out using a computer equipped with an Intel i7 quad-core processor with 3.4 GHz speed, 16 GB of RAM, and a fast-access solid-state drive (SSD). For modules 1 and 2, hyperparameters were obtained that characterize the estimation of the calibrated parameters and the discrepancy function, and consequently represent the GPs. These hyperparameters included a variance matrix $\sum$, a matrix of regression coefficient β, roughness parameters ω, and a noise variance matrix Λ, as explained in the methodology. Results of the calibrated parameters after applying the MBA in the undamaged state are illustrated in Figure 9 and Table 3. The posterior may require more data before it faithfully represents the calibrated parameters; as a result, it did not present any

changes compared with the prior. It is worth noting that the likelihood identified the calibrated parameters according to the measured data. As shown in Figure 9, in the undamaged state, there were no considerable changes in Young's moduli of the webs and the top slab in the likelihood against their priors. A significant change was observed in the reduction in the bottom slab's Young's modulus (E_{cBot}), which was identical to the observed minor cracks beneath the BGB. Another noticeable change was a reduction in vertical spring stiffness at the roller support, which infers that the vertical fixity at the roller support was overestimated. This outcome is well matched with the observed bouncing in the roller previously noticed in Figure 7.

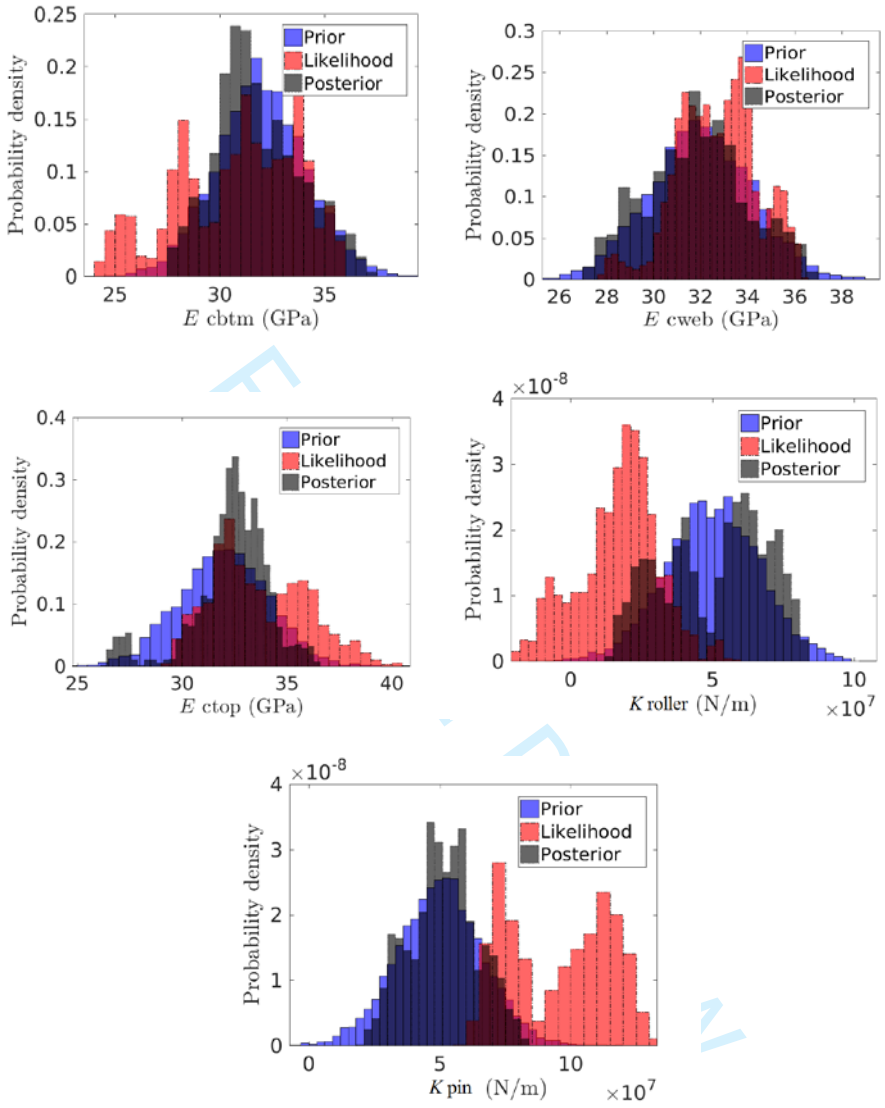

Figure 9. Prior, Max Likelihood and Posterior PDF for calibrated parameters in undamaged state.

Table 3. The Likelihood and Posterior distribution for calibrated parameters in undamaged state

	Posterior		Likelihood	
Part	Mean	Coefficient of Variation	Mean	Coefficient of Variation
E_{cBot}	31.81 (GPa)	4.1	30.84 (GPa)	8.3
E_{cWeb}	31.83 (GPa)	4.5	32.69 (GPa)	2.9
E_{cTop}	32.34 (GPa)	3.4	33.67 (GPa)	5.2
K_{Roller}	5.10×10^{7} (N/m)	3.32×10^{14}	1.68×10^{7} (N/m)	2.02×10^{14}
K_{Pin}	5.15×10^{7} (N/m)	1.66×10^{14}	9.53×10^{7} (N/m)	3.82×10^{14}

The discrepancy functions for all four modes in the undamaged state are depicted in Figure 10 (a). In this figure, the horizontal axis represents the sample ordering numbers of the simulated data. The black line represents the predicted mean, and the shaded region denotes a 95% prediction interval. As shown, the MBA predicted the measured responses accurately for all modes, with deviations of less than 6%.

Figure 10 (b) depicts the measured responses together with the prediction intervals for all four modal frequencies. The measured data points obtained from the experimental tests, as shown by red spots in Figure 10 (b), are randomly distributed among the simulated data points. As shown, the measured data points are located in the 95% prediction interval and are very close to the mean values of the predicted responses. The predicted mean values almost coincide with those of the measured data points for all modes (see Table 1). However, it can be inferred from the

predictions that the higher the mode order that is examined, the larger the scatter interval that is obtained.

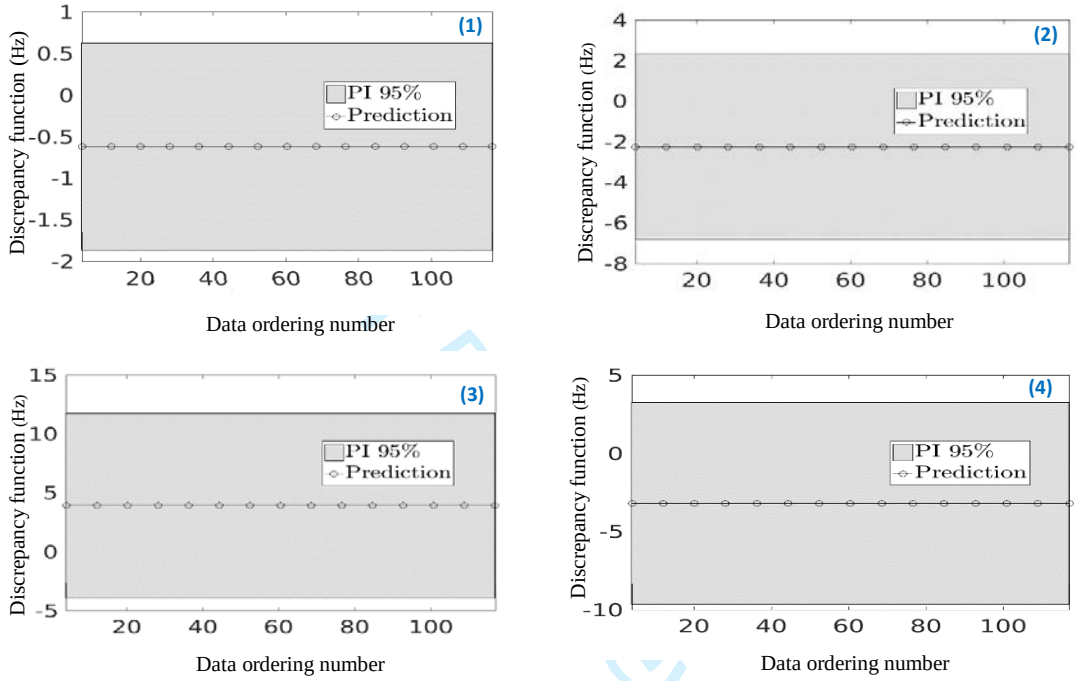

(a) Discrepancy functions for frequency responses.

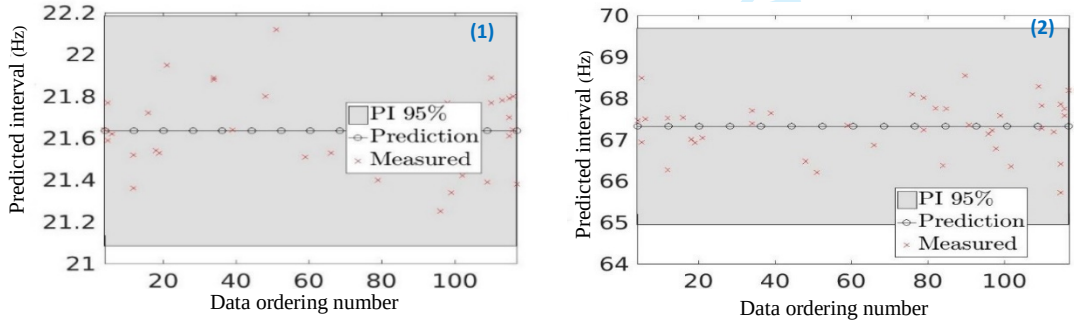

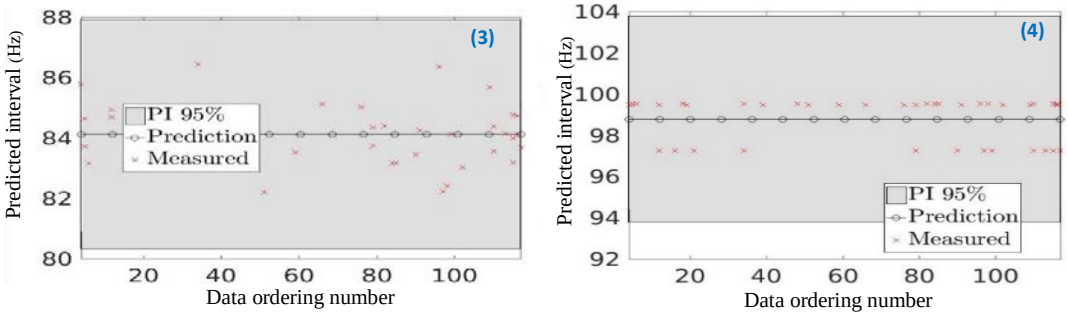

(b) Predicted interval 95% confidence for numerical model and experimental data points.

Figure 10. The results of Discrepancy function and predicted response for numerical model in undamaged state for all four modal frequencies as: (1) 1st vertical bending frequency, (2) 2nd vertical bending frequency, (3) 1st lateral bending frequency & (4) 3rd vertical bending frequency.

FEMU for damaged state

The next step of model updating refers to the damaged state, where some significant cracks were observed on the bottom slab and the webs of the BGB. It is worth mentioning that the number of calibrated parameters was reduced to three (Young's moduli) because it was assumed that the applying impacts in the damaged state did not affect the boundary conditions. Results of the prior, likelihood, and posterior distributions of the calibrated parameters are illustrated in Figure 11 and Table 4.

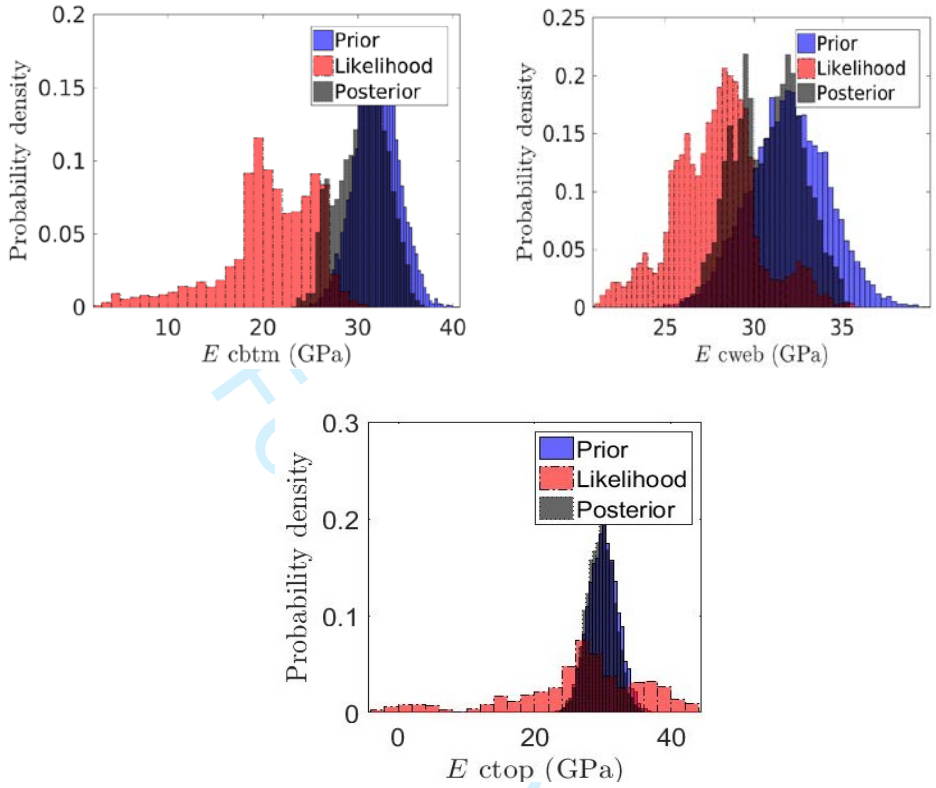

Figure 11. Prior, Max Likelihood and Posterior PDF for calibrated parameters in damaged state.

Table 4. The Likelihood and Posterior distribution for calibrated parameters in damaged state

	Posterior		Likelihood	
Part	mean	Coefficient of Variation	mean	Coefficient of Variation
E_{cBot}	30.45 (GPa)	6.45	20.63 (GPa)	25.59
E_{cWeb}	30.82 (GPa)	3.58	27.82 (GPa)	5.99
E_{cTop}	32.54 (GPa)	2.26	30.54 (GPa)	35.45

As shown in Figure 11, a significant change was targeted at the likelihood in Young's modulus of the bottom slab, indicating a reduction of about 35.5% to a new mean value of 20.63 GPa. Further, the decrease in Young's modulus of the web section was noticeable, showing a likelihood mean of 27 GPa. The impact forces had little effect on the top slab, and its updated Young's modulus was almost the same as its initial value. The reduction in the Young's moduli of the bottom slab and the webs is well matched with the cracks observed in the damaged state, as mentioned in the section *Two states of box girder bridge*. The discrepancy functions for all four modes in the damaged state are depicted in Figure 12 (a). As shown in the figure, the discrepancy increases in the damaged state, especially for the second and third vertical bending modes. In addition, the discrepancy functions in the damaged state are distributed more sparsely than those in the undamaged state. This may be because the cracks cause nonlinearities in the properties of structural materials and the mechanism of the experimental response.

Results of the measured responses together with predicted intervals for all four modes are shown in Figure 12 (b). As shown, the measured data points are observed in the corresponding predicted intervals and are very close to the mean values for all modes except the last one (third vertical bending mode). Results for the third vertical bending mode are very scattered. It is worth noting that the discrepancy of this mode is larger than that of the other modes, as shown in Figure 12 (b). This can

be explained because nonlinearity effects resulting from cracks become more significant when the vibration mode contains a higher-order curve.

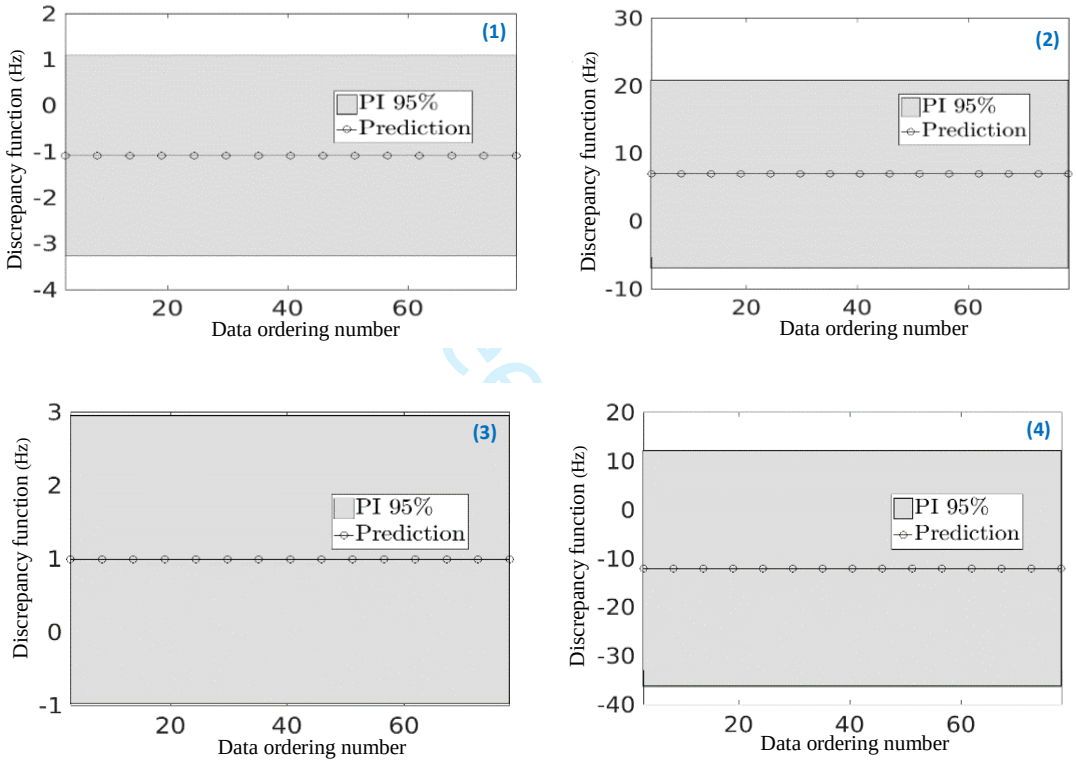

(a) Discrepancy functions for frequency responses.

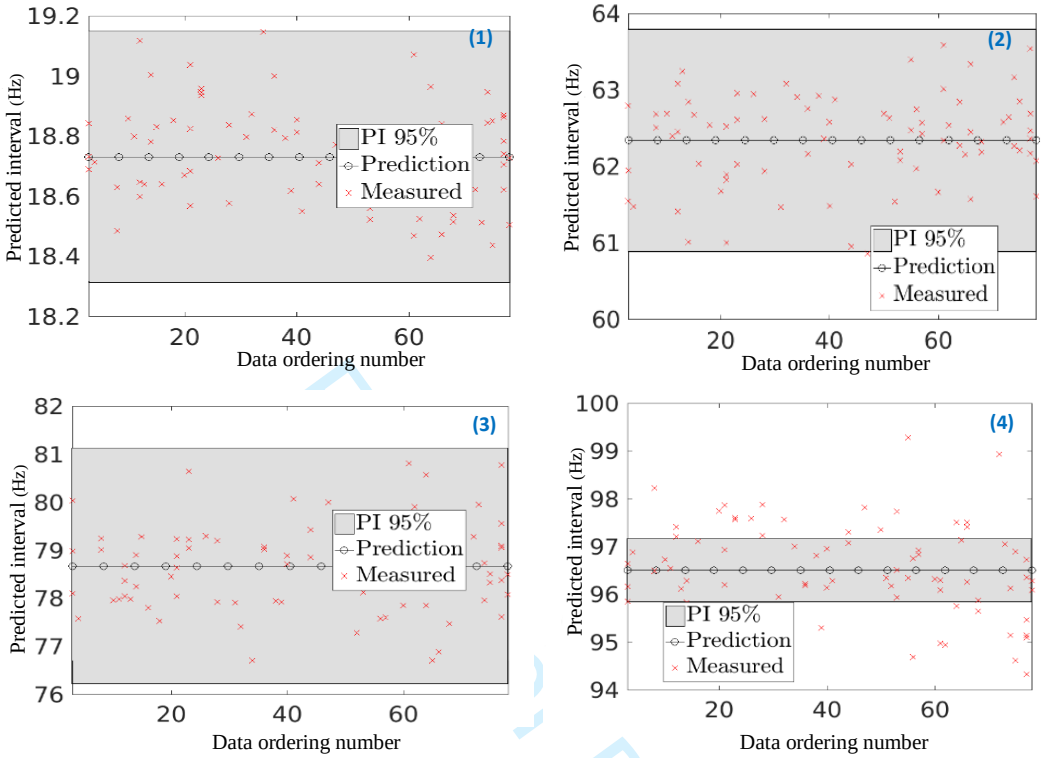

(b) Predicted interval 95% confidence for numerical model and experimental data points.

Figure 12. The results of discrepancy function and predicted response for numerical model in damaged state, for all four modal frequencies as: (1) 1st vertical bending frequency, (2) 2nd vertical bending frequency, (3) 1st lateral bending frequency & (4) 3rd vertical bending frequency.

Conclusions

In this study, the performance of an MBA was investigated in a large lab-scaled BGB using vibration data. Sensitivity analysis was conducted to select the most sensitive parameters and responses. Further, a metamodel was used instead of a

whole numerical model. Therefore, the computational task and processing time was reduced in comparison with other probabilistic updating techniques. This benefit distinguishes this approach, especially in applications to complex structures.

This study is the first to apply the MBA for two different states: damaged and undamaged. These two states represent the health conditions of the structure during its life span, and the outcomes can be used for further structural investigations. Although a case study is rather simple compared with full-scale real structures, such a scale provides a possibility to investigate the performance of the proposed approach in two different states according to the observed evidence on the structure. Further, this study highlighted the advantages of FEMU because it illustrated that even an FEM of a downscaled structure requires accurate calibration to be reliably used in further structural assessments.

Moreover, in contrast to many previous studies, which applied the MBA to a single parameter, this study investigated model updating on multiple parameters, such as material properties and boundary conditions, at the same time. In this study, the changes to these parameters were well matched with the observed evidence in both states. Natural frequencies of the first four modes, used as the measured data points, were predicted correctly. The updated model was sufficiently matched with the physical observation of the damaged structure. In turn, the results generated from

this study might be attributed to the proposed uncertainty quantification methodology. Further, as the results showed in the damaged state, the discrepancy functions increased, and experimental responses were not predicted as accurately as in the undamaged state. Such increases in the discrepancy functions are inferred as a guide for designers, implying that the FEM needs to be refined by considering additional aspects such as crack modeling. Further, response prediction can be improved and discrepancy can be reduced by adding other experimental data points (e.g., strain and mode shape) and information about environmental conditions (e.g., temperature and humidity). Although natural frequency was selected as the response for the updating process in this study, the MBA is capable of considering other types of responses. Thus, the performance of the approach when applied to other responses, such as mode shape, should be investigated in future studies. Consequently, the proposed methodology contributes to more reliable judgments about structural safety and more informed maintenance decision-making.

Acknowledgments

The first author would like to express his sincere appreciation to Queensland University of Technology (QUT) for the financial support for his research. The support provided by Australian Research Council (ARC) via a Discovery Project (DP160101764) is also gratefully acknowledged. Also, the support provided by technical support from FEMtools is acknowledged.

References

Arendt, P.D., Apley, D.W. and Chen, W (2012a) Quantification of model uncertainty: Calibration, model discrepancy, and identifiability. *Journal of Mechanical Design* 134(10):100908-100908-12.

Arendt, P.D., Apley, D.W., Chen, W., Lamb, D. and Gorsich, D (2012b) Improving identifiability in model calibration using multiple responses. *Journal of Mechanical Design* 134(10) 100909-100909-9.

Abaqus, F.E.A. (2017) Abaqus Inc. *Providence, Rhode Island, United States*.

Bayarri, M. J., Berger, J. O., Paulo, R., Sacks, J., Cafeo, J. A., Cavendish, J., Lin, C. H., and Tu, J (2007) "A Framework for Validation of Computer Models," *Technometrics* 49(2), pp. 138–154.

Beck, J.L. and Au, S.K. (2002) Bayesian updating of structural models and reliability using Markov chain Monte Carlo simulation. *Journal of engineering mechanics* 128(4), pp.380-391.

Beck, J.L. and Katafygiotis, L. S (1998) Updating models and their uncertainties. I: Bayesian statistical framework. *Journal of Engineering Mechanics* 124(4), pp.455-461.

Conde, B., Eguía, P., Stavroulakis, G.E. and Granada, E. (2018) Parameter identification for damaged condition investigation on masonry arch bridges using a Bayesian approach. *Engineering Structures* 172, pp.275-284.

Conti, S., Gosling, J.P., Oakley, J.E. and O'Hagan, A. (2009) Gaussian process emulation of dynamic computer codes. *Biometrika* 96(3), pp.663-676.

Darmawan, M.S. and Stewart, M.G. (2007) Spatial time-dependent reliability analysis of corroding pretensioned prestressed concrete bridge girders. *Structural Safety* 29(1), pp.16-31.

FEMtools UM (2012) *FEMtools Dynamic Design Solutions* N.V. (DDS)

Frangopol, D.M. (2011) Life-cycle performance, management, and optimisation of structural systems under uncertainty: accomplishments and challenges 1. *Structure and Infrastructure Engineering* 7(6), pp.389-413.

Friswell, M. and Mottershead, J.E. (2013) Finite element model updating in structural dynamics (Vol. 38). Springer Science & Business Media.

General principles on reliability for structures (AS 5104)

Higdon, D., Gattiker, J., Williams, B. and Rightley, M. (2008) Computer model calibration using high-dimensional output. *Journal of the American Statistical Association* 103(482), pp.570-583.

Jamali, S., Chan, T.H., Nguyen, A. and Thambiratnam, D.P. (2018) Reliability-based load-carrying capacity assessment of bridges using structural health monitoring and nonlinear analysis. *Structural Health Monitoring* 18(1), pp. 20–34.

Jamali, S., Chan, T.H., Thambiratnam, D.P., Pritchard, R. and Nguyen, A. (2016) Pre-test finite element modelling of box girder overpass-application for bridge condition assessment. In *Australasian Structural Engineering Conference: ASEC 2016* (p. 457). Engineers Australia.

Jesus, A., Brommer, P., Westgate, R., Koo, K., Brownjohn, J. and Laory, I. (2018) Bayesian structural identification of a long suspension bridge considering temperature and traffic load effects. *Structural Health Monitoring*
https //doi.org/10.1177/1475921718794299

Jesus, A., Brommer, P., Westgate, R., Koo, K., Brownjohn, J., & Laory, I. (2019) Modular Bayesian damage detection for complex civil infrastructure. *Journal of Civil Structural Health Monitoring* 1-15.

Jesus, A., Brommer, P., Zhu, Y. and Laory, I. (2017) Comprehensive Bayesian structural identification using temperature variation. *Engineering Structures* 141, pp.75-82.

Jesus, A.H., Dimitrovová, Z. and Silva, M.A. (2014) A statistical analysis of the dynamic response of a railway viaduct. *Engineering Structures* 71, pp.244-259.

Kennedy, M. and O'Hagan, A. (2001a) Bayesian calibration of computer models. *Journal of the Royal Statistical Society: Series B (Statistical Methodology)* 63(3), pp.425-464.

Kennedy, M. and O'Hagan, A. (2001b). Supplementary details on Bayesian calibration of computer. Rap. tech., University of Nottingham *Statistics Section*.

Li, H.N., Li, D.S., Ren, L., Yi, T.H., Jia, Z.G. and Li, K.P. (2016) Structural health monitoring of innovative civil engineering structures in Mainland China. *Structural Monitoring and Maintenance* 3(1), pp.1-32.

Liu, F., Bayarri, M.J. and Berger, J.O. (2009) Modularization in Bayesian analysis, with emphasis on analysis of computer models. *Bayesian Analysis* 4(1), pp.119-150.

Lophaven, S.N., Nielsen, H.B. and Søndergaard, J. (2002) *DACE: a Matlab kriging toolbox* (Vol. 2). IMM, *Informatics and Mathematical Modelling, the Technical University of Denmark.*

Mirza, S.A., Kikuchi, D.K. and MacGregor, J.G. (1980) Flexural strength reduction factor for bonded prestressed concrete beams. In *Journal Proceedings* (Vol. 77, No. 4, pp. 237-246).

Moravej H, Jamali S, Chan THT, Nguyen A. (2017) Finite element model updating of civil engineering infrastructures: a review literature. *International Conference on Structural Health Monitoring of Intelligent Infrastructure. Brisbane, Australia 2017.*

Mottershead, J.E., Link, M. and Friswell, M.I. (2011) The sensitivity method in finite element model updating: a tutorial. *Mechanical systems and signal processing* 25(7), pp.2275-2296.

O'Hagan, A. (2006) Bayesian analysis of computer code outputs: A tutorial. *Reliability Engineering & System Safety* 91(10-11), pp.1290-1300.

Pathirage TS. (2017). Identification of prestress force in prestressed concrete box girder bridges using vibration-based techniques. *Queensland University of Technology*.

Rasmussen, C. and Williams, C. (2006) Gaussian Processes for Machine Learning. *Adaptive Computation and Machine Learning*.

Shahidi, S.G. and Pakzad, S.N. (2013) Generalized response surface model updating using time domain data. *Journal of Structural Engineering* 140(8), p.A4014001.

Simoen, E., Papadimitriou, C. and Lombaert, G. (2013) On prediction error correlation in Bayesian model updating. *Journal of Sound and Vibration* 332(18), pp.4136-4152

Structural Vibration Solutions A/S (2011) SVS-ARTeMIS Extractor-Release 5.3, User's manual. Aalborg-Denmark

Weng, S., Xia, Y., Zhou, X.Q., Xu, Y.L. and Zhu, H.P. (2012) Inverse substructure method for model updating of structures. *Journal of Sound and Vibration* 331(25), pp.5449-5468.